THE USE OF BROADBAND SIGNALS FOR UNDERWATER ACOUSTIC TRANSDUCER CALIBRATION

A. Zed Robinson, Jr., et al

Naval Research Laboratory
Washington, D. C.

17 April 1975

UNCLASSIFIED
SECURITY CLASSIFICATION OF THIS PAGE *(When Data Entered)*

REPORT DOCUMENTATION PAGE		READ INSTRUCTIONS BEFORE COMPLETING FORM
1. REPORT NUMBER NRL Report 7883	2. GOVT ACCESSION NO.	3. RECIPIENT'S CATALOG NUMBER AD-A008 324
4. TITLE *(and Subtitle)* THE USE OF BROADBAND SIGNALS FOR UNDERWATER ACOUSTIC TRANSDUCER CALIBRATION		5. TYPE OF REPORT & PERIOD COVERED An interim report on the NRL continuing problem 6. PERFORMING ORG. REPORT NUMBER
7. AUTHOR(s) A. Zed Robinson, Jr. L. G. Beatty		8. CONTRACT OR GRANT NUMBER(s)
9. PERFORMING ORGANIZATION NAME AND ADDRESS Naval Research Laboratory Underwater Sound Reference Division P. O. Box 8337, Orlando, Fla. 32806		10. PROGRAM ELEMENT, PROJECT, TASK AREA & WORK UNIT NUMBERS NRL Problem S02-37 Project No. RR 011-08-41
11. CONTROLLING OFFICE NAME AND ADDRESS Department of the Navy Office of Naval Research Arlington, Va. 22217		12. REPORT DATE 17 April 1975 13. NUMBER OF PAGES iv + 57
14. MONITORING AGENCY NAME & ADDRESS*(if different from Controlling Office)*		15. SECURITY CLASS. *(of this report)* UNCLASSIFIED 15a. DECLASSIFICATION/DOWNGRADING SCHEDULE NA

16. DISTRIBUTION STATEMENT *(of this Report)*

Approved for public release; distribution unlimited.

17. DISTRIBUTION STATEMENT *(of the abstract entered in Block 20, if different from Report)*

18. SUPPLEMENTARY NOTES

19. KEY WORDS *(Continue on reverse side if necessary and identify by block number)*

Underwater acoustic transducer calibration
Broadband techniques
Fourier transforms
Digital systems
Signal Averaging
Computer data reduction
Power spectral density
Spectral smoothing (continued)

20. ABSTRACT *(Continue on reverse side if necessary and identify by block number)*

A preliminary study of the potential use of broadband signals for underwater acoustic transducer calibration has been made. Emphasis was placed on pulses of a single cycle of a sinusoidal wave as the calibration signal. The experiments involved digital sampling of the current and voltage response waveforms, generating the Fourier transforms of these responses, and combining the transforms to provide the desired calibration curves. The results were considered comparable to those obtained with conventional operational systems, even (continued)

DD FORM 1 JAN 73 1473 EDITION OF 1 NOV 65 IS OBSOLETE
S/N 0102-014-6601

UNCLASSIFIED
SECURITY CLASSIFICATION OF THIS PAGE *(When Data Entered)*

19. KEY WORDS (continued):

Probability density functions
Cumulative probability distributions

20. ABSTRACT (continued):

though smoothing was not applied to the data and even though compromises were required in performing the experiments. Preliminary noise analyses included the development of certain useful probability density functions and cumulative probability distribution functions. Curves to illustrate these probability functions are plotted. Some interpretation of noise effects is given. Future research plans are described briefly.

ERRATA

NRL Report 7883

Page 46, change the expression that follows Eq. (B19) to read:

$$Q(u,y,A) = \{2 \arcsin u/\sqrt{y^2 + (A - u)^2}\}^{-1} \text{ for } \ldots$$

Page 48, change the last term of Eq. (B21) from da to dA.

Contents

Figures (continued):

Tables:

THE USE OF BROADBAND SIGNALS FOR UNDERWATER ACOUSTIC TRANSDUCER CALIBRATION

Introduction

The response of a system to a standard input signal is one of the earliest methods used to characterize linear systems. Such a concept was first proposed by George Green in "An Essay on the Application of Mathematical Analysis to the Theories of Electricity and Magnetism" presented in 1838; consequently, such responses often are referred to as Green's functions. Stedman [1] published an expository paper (1968) on the current widespread use of Green's functions as an analytical technique for linear systems in several physical disciplines, including electronic systems, mechanical systems, optical systems, and electrostatic systems. The technique is applicable in any invariant linear system where causality exists--that is, no output exists without a prior input.

The most common standard inputs are the unit impulse function and the unit step function. It is common today to refer to the system's response to a unit impulse function as the Green's function and to the system's response to a unit step function as the indicial admittance. A relatively early text by Goldman [2] published in 1949 gives a good treatment of the use of Green's functions and the indicial admittance as analytical tools for electrical transients. In this report, the terms "system impulse response" and "system step-function response" will be used to avoid possible confusion.

Although both the system impulse response and the system step-function response describe a linear system, the more commonly used characterization is the system transfer function. There is an implicit assumption of a two-port system relationship here; however, the concepts may be applied in a completely general sense. The system transfer function (in a Fourier-related sense) is the amplitude and phase responses of the system to a steady-state sinusoidal input as a function of the frequency of the input.

All of the different forms of system characterizations are directly derivable one from the other. For example, the transfer function is the Fourier transform of the system impulse response.

A similar type of transfer function is that derived by taking the Laplace transform of the system impulse response. In many cases, using

this function allows the system to be characterized by a pole-zero plot in the complex domain; however, the primary concern in this report will be Fourier transform methods and, unless otherwise specified, the system transfer function will mean the Fourier-related transfer function.

The system transfer functions may also be derived from types of standard inputs other than the steady-state sinusoidal input; however, indeterminate values of the transfer function will exist for those frequencies for which the value of the Fourier transform of the input is zero.

Almost all of the past methods for calibrating underwater acoustic transducers have involved a direct measurement of the amplitude response to a steady-state sinusoidal input. There has been little interest in the phase response. Both "sweep-frequency" and/or "pulsed c-w" methods have been used, but the sweep rate and pulse length have been such that the steady-state condition was approximated before measurements were made. Although the potential usefulness of a broadband signal for underwater acoustic transducer calibration has long been known, very little has been done to explore this potential. An exception is work by Osborne and Carter [3] in 1946 involving the use of underwater explosions as calibration sources. One of the problems at that time was the practical difficulty in deriving the transfer function from the temporal measurements. In recent years, however, the rapid development of high-speed digital computers along with fast Fourier transform algorithms has all but eliminated this difficulty. For example, Hohmann and Louden [4] have applied this technique to the calibration of transducers in air.

The authors believe that using broadband signals for acoustic calibration potentially provides a faster method of calibration than the c-w sweep-frequency procedures now in common use. They also believe that future calibration requirements will include the need for phase response as well as amplitude response for transducers. This latter belief is based on the greatly increasing number of sonar systems that depend on broadband signals and coherent detection. The use of broadband calibration signals should greatly facilitate the measurement of phase response.

Theory

General Fourier transform theory, its applications to acoustical problems, and the use of digital and computer techniques in its application are described in a number of texts [5-12]. Because there are differences in conventions adopted by various authors, some of the more important definitions and relationships will be stated here. The Fourier transform of g(t) is defined as

$$G(f) = \int_{-\infty}^{\infty} g(t)e^{-j2\pi ft}dt; \qquad (1)$$

consequently, g(t) may be expressed as

$$g(t) = \int_{-\infty}^{\infty} G(f)e^{j2\pi ft}df. \tag{2}$$

If g(t) is applied as the input to a linear system with an impulse response function h(t), the output of that system is given by

$$m(t) = \int_{-\infty}^{\infty} h(\tau)g(t - \tau)d\tau, \tag{3}$$

or the system output is given by the convolution of the system impulse response and the system input. If causality exists and if g(t) is assumed to be zero for negative t, Eq. (3) becomes

$$m(t) = \int_{0}^{t} h(\tau)g(t - \tau)d\tau. \tag{4}$$

The Fourier transform of m(t) is given by

$$M(f) = W(f)G(f), \tag{5}$$

where W(f) is the complex transfer function of the system and is also the Fourier transform of the system impulse response. In Fourier transform theory, the multiplication process in the frequency domain is equivalent to convolution in the time domain and, conversely, convolution in the frequency domain is equivalent to multiplication in the time domain. If two linear systems are cascaded so that the output of the first serves as the input to the second, the output of the second is equal to the double convolution of the input with the two system impulse response functions. On the other hand, the Fourier transform of the output is the product of the Fourier transform of the input and the two system complex transfer functions. For this reason, it is generally more desirable to work in the frequency domain when cascading of linear systems is involved.

Another useful concept is the autocorrelation function of a signal, which is defined (in a temporal sense) as

$$\phi_{11}(\tau) = \lim_{T\to\infty} \frac{1}{T} \int_{-\frac{1}{2}T}^{\frac{1}{2}T} g_1(t)g_1(t - \tau)dt. \tag{6}$$

The power spectral density of $g_1(t)$ is defined as

$$P_{11}(f) = \lim_{T\to\infty} \frac{G_1(f)G_1^*(f)}{T}, \tag{7}$$

where $G_1^*(f)$ is the complex conjugate of $G_1(f)$. The autocorrelation function and the power spectral density are Fourier transform pairs by the Wiener-Khintchine theorem. In an analogous manner, the cross-correlation function of $g_1(t)$ and $g_2(t)$ is defined as

$$\phi_{12}(\tau) = \lim_{T\to\infty} \frac{1}{T} \int_{-\frac{1}{2}T}^{\frac{1}{2}T} g_1(t) g_2(t - \tau) dt, \tag{8}$$

and the cross-power spectral density of $g_1(t)$ and $g_2(t)$ is defined as

$$P_{12}(f) = \lim_{T\to\infty} \frac{G_1(f) G_2^*(f)}{T}. \tag{9}$$

Again, by the Wiener-Khintchine theorem, the cross-correlation function and the cross-power spectral density function are Fourier transform pairs. Note that although the autocorrelation function must be an even-valued function, this is not true for the cross-correlation function. Likewise, the power spectral density function must be real and positive for all values of f, but the cross-power spectral density function may be complex.

Before applying these relationships to underwater acoustic transducer calibration, the reader is referred to Bobber [13] for an excellent treatment of acoustic calibration methods and techniques. Two methods of calibration will be discussed. The first method is comparison calibration in which the response of an unknown transducer is obtained by comparing it to that of a calibrated standard. The second is the reciprocity calibration method, which is an absolute calibration procedure. Figure 1 is a block diagram of a typical underwater acoustic transducer calibration set-up where broadband calibration signals might be used. The signal generator produces a broadband standard signal that provides an input to the power amplifier, which drives a projector. The projector S, in response to a driving current i(t), generates a sound pressure at the hydrophone that produces the output $e_1(t)$. With capital letters used to denote Fourier transforms of the time functions and assuming a noise-free unbounded linear condition, $e_1(t)$ may be expressed in the frequency domain as

$$E_1(f) = I_1(f) S(f) M_1(f), \tag{10}$$

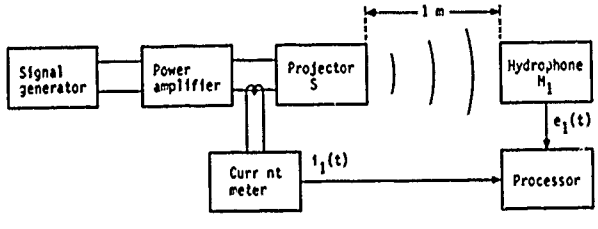

Fig. 1. Typical arrangement for underwater acoustic transducer calibration.

where $S(f)$ and $M_1(f)$ represent, respectively, the transmitting current response of the projector and the free-field (open-circuit) voltage sensitivity of the hydrophone. If the complex free-field voltage sensitivity (receiving response) of M_1 is known, then a comparison calibration may be achieved for an unknown hydrophone M_2 by first performing the experiment with the known hydrophone M_1 and calculating the Fourier transforms of $i_1(t)$ and $e_1(t)$. The exact same experiment then is repeated with hydrophone M_1 replaced by the unknown hydrophone M_2, and the Fourier transforms of $e_2(t)$ and $i_2(t)$ are computed. The Fourier transform of $e_2(t)$ is given by

$$E_2(f) = I_2(f)S(f)M_2(f). \tag{11}$$

The complex receiving response of M_2 then is obtained by combining Eqs. (10) and (11) to give

$$M_2(f) = M_1(f) \frac{E_2(f)}{I_2(f)} \frac{I_1(f)}{E_1(f)}. \tag{12}$$

If only the amplitude response of M_1 is known, then the amplitude response of M_2 is given by

$$|M_2(f)| = |M_1(f)| \frac{|E_2(f)|}{|I_2(f)|} \frac{|I_1(f)|}{|E_1(f)|}. \tag{13}$$

Equations (12) and (13) will provide calibration results for all frequencies except where $I_1(f)$, $I_2(f)$, or $S(f)$ goes to zero. There is an implicit assumption that the projector S is linear; however, the effect of a nonlinear projector may be largely overcome by insuring that $i_1(t)$ and $i_2(t)$ are the same. Equation (12) then becomes

$$M_2(f) = M_1(f) \frac{E_2(f)}{E_1(f)}. \tag{14}$$

An equivalent approach to achieve the same results is the use of the cross-correlation function. In this case, with the known (or standard) hydrophone M_1 in the experiment, an estimate of the cross-correlation function of $i_1(t)$ and $e_1(t)$ is calculated by

$$\phi_{ie}^{(1)}(\tau) \doteq \frac{1}{T} \int_0^T i_1(t)e_1(t - \tau)dt. \tag{15}$$

An estimate of the cross-power spectral density of $i_1(t)$ and $e_1(t)$ then is obtained by taking the Fourier transform of the cross-correlation function to give

$$\text{F.T.}[\phi_{ie}^{(1)}(\tau)] \doteq \frac{I_1(f)E_1^*(f)}{T} \doteq \frac{I_1(f)I_1^*(f)S^*(f)M_1^*(f)}{T} . \tag{16}$$

If this procedure is repeated with the unknown hydrophone M_2 in the experiment, then

$$\text{F.T.}[\phi_{ie}^{(2)}(\tau)] \doteq \frac{I_2(f)E_2^*(f)}{T} \doteq \frac{I_2(f)I_2^*(f)S^*(f)M_2^*(f)}{T} \tag{17}$$

is obtained. Combining Eqs. (16) and (17) gives

$$M_2^*(f) = M_1^*(f) \frac{|I_1(f)|^2}{|I_2(f)|^2} \frac{\text{F.T.}[\phi_{ie}^{(2)}(\tau)]}{\text{F.T.}[\phi_{ie}^{(1)}(\tau)]}. \tag{18}$$

If $i_1(t)$ and $i_2(t)$ are the same in both experiments, then

$$M_2^*(f) = M_1^*(f) \frac{\text{F.T.}[\phi_{ie}^{(2)}(\tau)]}{\text{F.T.}[\phi_{ie}^{(1)}(\tau)]}. \tag{19}$$

This cross-correlation function is likely to be more useful when the broadband calibration signal is a continuous one, such as pseudorandom noise; the first approach is likely to be more useful with broadband transient signals.

The previous paragraphs have dealt exclusively with comparison-type calibrations for which a standard hydrophone was available. The procedures also concerned only the measurement of hydrophone free-field voltage sensitivity, given the calibrated standard It should be obvious that measurement of the transmitting response of a linear projector, given the same standard hydrophone, is even simpler, requiring only a single experiment.

Bobber [13] describes several methods of absolute calibration, the most important of which is the reciprocity method. The experimental procedures are exactly the same as those described in the previous paragraphs, except that a transducer known to obey the reciprocity principle must be available and the experiments must be conducted three different times in identical manners--once as in Fig. 1 with the projector S and the hydrophone M; a second time with the reciprocal transducer R used in place of the projector; and a third time with the reciprocal transducer used in place of the hydrophone. Taking the Fourier transforms of the driving currents and the output voltages yields the following equations:

$$
\begin{aligned}
&\text{(S-M):} \quad E_{MS}(f) = I_{SM}(f)S(f)M(f), \\
&\text{(R-M):} \quad E_{MR}(f) = I_{RM}(f)R_T(f)M(f), \\
&\text{(S-R):} \quad E_{RS}(f) = I_{SR}(f)S(f)R_R(f),
\end{aligned} \tag{20}
$$

where $R_t(f)$ is the transmitting current response of the reciprocal transducer and $R_R(f)$ is the free-field (open-circuit) voltage sensitivity of the reciprocal transducer. Now, the reciprocity parameter is defined as

$$
J(f) = \frac{R_R(f)}{R_T(f)}. \tag{21}
$$

Combining Eqs. (20) and (21) produces an absolute calibration for all of the acoustic devices. For example, the free-field voltage sensitivity of the hydrophone is given by

$$
M(f) = \left[\frac{E_{MR}(f)E_{MS}(f)I_{SR}(f)}{I_{RM}(f)I_{SM}(f)E_{RS}(f)} J(f)\right]^{1/2}. \tag{22}
$$

If $i_{SR}(t) = i_{SM}(t)$, then Eq. (22) becomes

$$
M(f) = \left[\frac{E_{MR}(f)E_{MS}(f)}{I_{RM}(f)E_{RS}(f)} J(f)\right]^{1/2}, \tag{23}
$$

which is equivalent to Bobber's [13] Eq. (2.17).

The reciprocity parameter is discussed extensively by Bobber [13]. Bobber also discusses [14] the development of a generalized reciprocity parameter. Past underwater acoustic transducer calibrations have dealt only with amplitude functions (in almost all cases); therefore, the reciprocity parameter usually has been treated as a real function. If complex responses are required in an acoustic calibration, a complex reciprocity parameter is needed. Beranek [15] has derived such a complex spherical reciprocity parameter for spherical waves where complete spherical symmetry exists. The same parameter is derived in a slightly different form in Appendix A. Using this derivation, Eq. (23) becomes

$$
M(f) = \left[-j \frac{E_{MR}(f)E_{MS}(f)}{I_{RM}(f)E_{RS}(f)} \frac{2}{f\rho_0} e^{j2\pi f/c}\right]^{1/2}, \tag{24}
$$

when the transducers are separated by 1 m during the measurements

If the method of processing is to be that involving the cross-correlation functions of transducer driving currents and transducer

response voltages, then Eq. (20) for the three experiments becomes

$$\begin{aligned} \text{F.T.}[\phi_{SM}(\tau)] &= |I_{SM}(f)|^2 S^*(f) M^*(f), \\ \text{F.T.}[\phi_{RM}(\tau)] &= |I_{RM}(f)|^2 R_T^*(f) M^*(f), \\ \text{F.T.}[\phi_{SR}(\tau)] &= |I_{SR}(f)|^2 S^*(f) R_R^*(f), \end{aligned} \tag{25}$$

where the first subscript indicates the transducer used as the projector and the second subscript indicates the one used as the receiver. Combining Eq. (25) with Eq. (21) and assuming that $I_{SM}(f) = I_{SR}(f)$ gives

$$M^*(f) = \left(\frac{\text{F.T.}[\phi_{RM}(\tau)] \cdot \text{F.T.}[\phi_{SM}(\tau)]}{\text{F.T.}[\phi_{SR}(\tau)] \cdot |I_{RM}(f)|^2} J^*(f) \right)^{\frac{1}{2}}, \tag{26}$$

The advantage of this processing method is in the use of continuous broadband calibration signals where truncation methods (to be described later) can be used to discriminate against multipath arrivals at the receiver.

Noise Analysis and Discrimination

The theory discussed in the previous section has dealt with acoustic transducer calibration under conditions that are highly idealized by assuming the existence of a free field, absolute accuracy in measurements, and no contaminating noise sources.

The absence of free-field conditions may be compensated in two ways: (1) by keeping the separation between projector and hydrophone small (consistent with near-field constraints) during calibration measurements so that the levels of multipath signals are small in comparison with the level of the direct signal, and (2) by truncation of the signal in the time domain. The first of these procedures is common to all calibration methods; the second applies only to broadband signals. In the case of a broadband transient signal, the truncation occurs directly in the time domain with the signal designed as nearly as possible to insure that effects due to the direct arrival have diminished to zero before the first multipath signal arrives. In the case of broadband continuous noise, the truncation occurs on the correlation function that is calculated. Again the signal design should be such that the correlations due to direct and multipath signals are resolvable. Truncation of the signals in this manner will have an effect on the character of the noise and on the ability to achieve absolute accuracy in the measurements. This effect will be discussed briefly in subsequent paragraphs.

Absolute accuracy in acoustic measurements never is completely achievable, partly because of the lack of exact calibrations of the

measuring instruments, but mostly because of contaminating noise that introduces errors in the measurements. Noise in the measuring system comes from various sources, the most notable being the ambient noise that exists in the calibration enclosure. Another source of noise is the electronic measuring system itself. Also of importance is noise induced in the system by the kind of processing being used, particularly for digital systems, which contain sampling noise due to discrete samples in time. There is also quantization noise due to discrete quantization levels, as well as errors introduced by such things as signal truncation and finite sample sizes. In the calibration methods described in this report, extreme care must be given to each source of error, because often what appears to be a small error can be magnified many times in the final result.

In most measurement problems, it is appropriate to start with an analysis of the largest source of error and determine how best to treat it before moving to the next most important source. In the underwater acoustic calibration problem, this source is the ambient noise in the calibration enclosure. The output voltage of the hydrophone in Fig. 1 would be

$$\widehat{e_1(t)} = e_1(t) + m_1(t), \tag{27}$$

where $e_1(t)$ is the output that is generated by the acoustic field produced by the projector, $m_1(t)$ is the output due to the ambient noise field, and $\widehat{e_1(t)}$ is the measured output of the hydrophone.

One rather obvious way to discriminate against this kind of noise is to use signal averaging; that is, repeat the calibration experiment many times in a manner such that signals will add coherently while the noise adds incoherently. If the signals are all completely coherent and the noise samples are independent, the gain in signal-to-noise ratio (expressed in decibels) is 10 log n, where n is the number of experimental outputs used in the average. It should be clear that a price is paid in terms of time required for the total calibration in this kind of noise discrimination. For example, 100 experiments will give a signal-to-noise improvement of 20 dB, but an additional 100 experiments will be required for a further improvement to 23 dB; that is, an improvement of 3 dB requires a doubling of time required for the total calibration.

This kind of signal averaging is also generally effective against types of noise other than the ambient noise field in the calibration enclosure. For example, it will be effective against electronic noise associated with the preamplifier for the hydrophone and against electrical noise associated with inadequate grounding or actual electrical response of the hydrophone to electrical signals in the water. Signal averaging will be effective also against quantizing noise associated with digitizing $e_1(t)$, provided that rounding of the average is not used and that the sampling is not synchronous with the signal. For instance,

if 100 samples of data are taken and digitized with a 1-mV quantization level, the effective quantization level without rounding for the averaged signal would be 0.01 mV. Actually the quantization noise is completely dependent on the final effective quantization level, which usually can be controlled so that it presents no measurement problem.

Signal averaging will not be effective against signal-induced noise such as multipath interference or electrical crosstalk in the system. Neither will it be effective against bias-type measurement errors.

For a more detailed analysis of the effect of random (or incoherent) noise, consider the result of 100 experiments in which the data have been digitized and signal averaging has been applied. Antialiasing filters are assumed to have been used prior to the digitizing to eliminate any aliasing effects. The results may be written as

$$\widehat{e_1(k\Delta t)} = e_1(k\Delta t) + m_1(k\Delta t), \tag{28}$$

where k is the number of samples, $1/\Delta t$ is the sampling rate used, $\widehat{e_1(k\Delta t)}$ is the digitized and averaged output, $e_1(k\Delta t)$ is that part of $\widehat{e_1(k\Delta t)}$ due to the acoustic field produced by the projector, and $m_1(k\Delta t)$ is that part of $\widehat{e_1(k\Delta t)}$ produced by a combination of ambient noise, electronic noise, and quantization noise. It is desired that the power spectral density of the output be estimated by taking the discrete Fourier transform (DFT) of $\widehat{e_1(k\Delta t)}$. For processing efficiency, it is desirable that the number of samples k be equal to 2^n so that one of the standard fast Fourier transform (FFT) algorithms can be used to generate the DFT. The DFT can be thought of as a digital analog of the Fourier series expansion of a function, therefore any particular Fourier component may be written as

$$u \cos(\omega_\ell t + \theta) = A \cos \omega_\ell t + x \cos(\omega_\ell t + \phi), \tag{29}$$

where u is the measured value of the amplitude of the Fourier component, A is the amplitude of the Fourier component due to the signal, x is the amplitude of the Fourier component due to the noise, and ϕ is the phase difference between the Fourier components due to the signal and the noise. Because the original signal and noise are independent variables, ϕ will be a random variable with a uniform distribution. The noise may be assumed to have a Gaussian distribution, particularly after the averaging (where the average tends toward a Gaussian distribution because of the Central Limit Theorem). The conditional distribution density of u, given A, then can be expressed by the Rician [9] distribution density

$$p(u|A) = (u/\sigma^2)\{\exp[-(u^2 + A^2)/2\sigma^2]\}I_0(uA/\sigma^2), \tag{30}$$

where u is the measured value of the amplitude of the Fourier component, A is the amplitude of the Fourier component due to the signal, σ^2 is the variance of the noise variable (after averaging), and $I_0(uA/\sigma^2)$ is the modified Bessel function of zero order with the argument uA/σ^2. An integral expression [15] for the modified Bessel function of zero order is given by

$$I_0(z) = (1/\pi) \int_0^{\pi} e^{z \cos \theta} \, d\theta, \tag{31}$$

so that Eq. (30) may be rewritten as

$$p(u|A) = (u/\sigma^2)\{\exp[-(u^2 + A^2)/2\sigma^2]\}(1/\pi) \int_0^{\pi} \exp[(uA/\sigma^2)\cos \theta]d\theta$$

$$= (u/\sigma^2)\{\exp[-(u^2 + A^2)/2\sigma^2]\}(1/\pi) \int_0^{\pi} \exp[(uA/\sigma^2)(1 - 2 \sin^2 \tfrac{1}{2}\theta)]d\theta$$

$$= (u/\sigma^2)\{\exp[-(u - A)^2/2\sigma^2]\}(2/\pi) \int_0^{\frac{1}{2}\pi} \exp[(-2uA/\sigma^2)\sin^2\phi]d\phi. \tag{32}$$

Equation (32) is a somewhat better expression for generating the distribution density function by numerical integration. It also can be used to show how the distribution approaches a Rayleigh distribution as A approaches zero and how it approaches a Gaussian distribution as A becomes large in comparison with σ.

For calculation, it is desirable to express both u and A in units of σ (that is, let $\sigma = 1$) so that Eq. (32) becomes

$$p(u|A) = u\{\exp[-\tfrac{1}{2}(u - A)^2]\}(2/\pi) \int_0^{\frac{1}{2}\pi} \exp(-2uA \sin^2\phi)d\phi. \tag{33}$$

This distribution density is plotted in Fig. 2 for the values A = 1,3,5.

The cumulative form of the Rician distribution density is useful for the noise analysis of this report. It is obtained by taking the integral of Eq. (32); that is,

$$p(u<x|A) = \int_0^{x} p(u|A)du. \tag{34}$$

This distribution is plotted in Fig. 3 for $\sigma = 1$ and for A = 1,3,5.

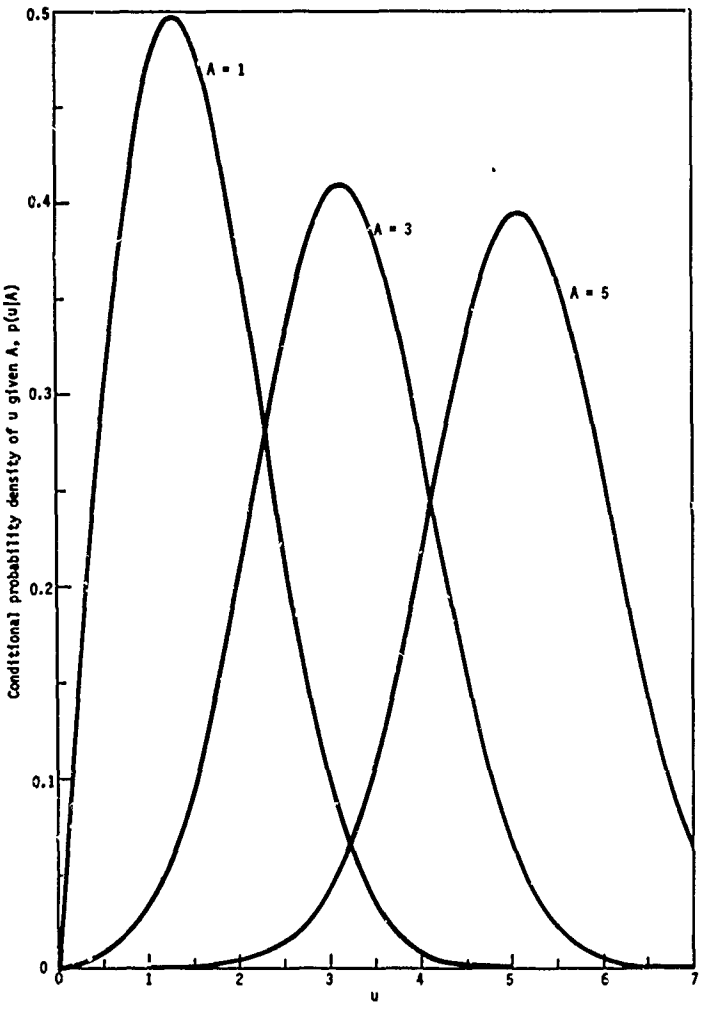

Fig. 2. Examples of Rician distribution density for $\sigma = 1$, as calculated from Eq. 33.

The usefulness of the distribution shown in Fig. 3 is in determining the errors introduced by the noise in the measurement of the amplitude of the Fourier transform of a given signal, particularly where the transform is generated on a point-by-point basis. With a known value A of the Fourier component of the signal and with a known statistic σ^2 of the noise, the cumulative distribution of the measured value of the amplitude of a single Fourier component is given by Fig. 3; that is, if the experiment were repeated an infinite number of times, the cumulative distribution of the measured value u, given A and σ^2, would be that shown by Fig. 3. For example, from Fig. 3 for A = 5 (or +14 dB above the noise level), the probability of a measured value of u being less than 3.75 (-2.5 dB re A) is 0.085. Likewise, the probability of a measured value of u being greater than 6.67 (+2.5 dB re A) is 0 057. Therefore, the probability of an absolute error in a single measurement of u being greater than 2.5 dB is 0.142. For measured values of u for

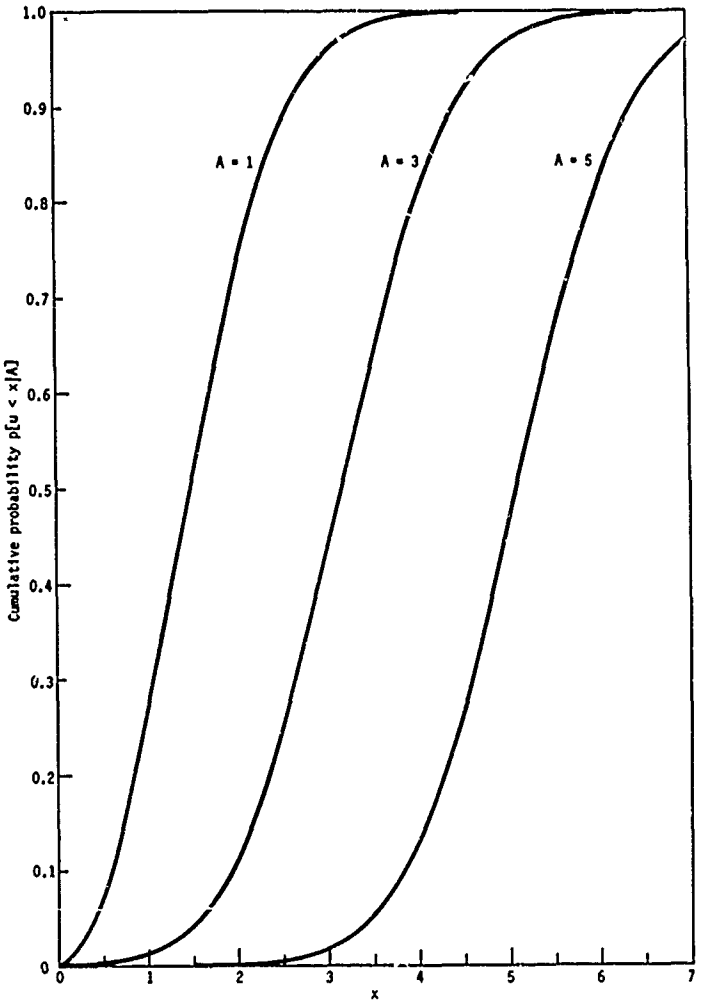

Fig. 3. Cumulative form of Rician distribution for $\sigma = 1$ and $A = 1,3,5$.

different frequency points in a given spectrum (for A = +14 dB above the noise) where the errors for the different points are independent, an error of 2.5 dB or greater will occur on the average of 1 in 7 points. This fact illustrates the need for smoothing the amplitude spectra before using them in the calibration calculation. The type of smoothing required should not be confused with conventional smoothing such as Hann, Hamming, or Parzen windows. Although these smoothing methods may be useful, they are primarily aimed at giving a best estimate of spectra based on limited discrete samples of the original time series. They do not take into consideration the fact that undesired noise may be contaminating the original time series.

Information on the type of spectral smoothing that will be desirable in underwater acoustic transducer calibration procedures has not yet been developed. Possibilities exist for segmenting the raw spectrum and doing a least-squares fit to a quadratic or cubic for each segment with a matching of end points. Consideration should be given also to individual

smoothing of the real and imaginary parts of the spectrum before they are combined to give the amplitude spectrum. The problem of spectrum smoothing will be one important phase of future work.

Also of importance in the noise analysis is the cumulative distribution of the quotient of two Rician variables. This distribution becomes important because of the need to take the quotient of measured spectral densities in the underwater acoustic calibration procedure. The distribution of a single point in the resultant spectral curve is given by the quotient of two Rician variables and can be expressed in a cumulative form as the conditional probability of $u_1/u_2 < x$, given A_1, A_2, σ_1, and σ_2. For a given value of u_2, the probability of u_1/u_2 being less than x is simply the probability of u_1 being less than xu_2. If the errors associated with the measurements of u_1 and u_2 are independent, the desired cumulative distribution may be calculated by simply integrating the product of the probability density of u_2 and the probability of u_1 being less than xu_2 over all values of u_2. This cumulative distribution of the quotient is expressed in integral form by

$$p(u_1/u_2<x|A_1;A_2;\sigma_1;\sigma_2) = \int_0^\infty p(u_2|A_2;\sigma_2)p(u_1<xu_2|A_1;\sigma_1)du_2$$

$$= \int_0^\infty p(u_2|A_2;\sigma_2)\left[\int_0^{xu_2} p(u_1|A_1;\sigma_1)du_1\right]du_2, \qquad (35)$$

where $p(u_i|A_i;\sigma_i)$ is given by Eq. (32). This cumulative distribution is plotted in Fig. 4 for values of $\sigma_1 = \sigma_2 = 0$ dB and $A_1 = A_2 = 10$ dB, 15 dB, 20 dB, and 30 dB. The decibel scale has been used in the plots to facilitate analyses of errors. For example, for $A_1 = A_2 = 20$ dB, $\sigma_1 = \sigma_2 = 0$ dB, the probability that the error in the measured value of u_1/u_2 will be greater than 1.6 dB is 0.2. Also, the probability of the error in u_1/u_2 (for $A_1 = A_2 = 30$ dB) being greater than 0.5 dB is 0.2. This fact further illustrates the need for smoothing either in the spectral estimates or in the generation of the final calibration curves, or both.

In addition to the Rician distribution, another distribution of general interest in calibration problems is the probability of A, given the measured value of u and the noise statistics. This distribution is of particular value in parameter estimation and the establishment of confidence limits for relatively small signal-to-noise ratios. A derivation of this probability density function, referred to as a modified

Rician distribution, is given in Appendix B. A derivation of the distribution of A_1/A_2, given u_1 and u_2 and the two noise statistics, is also given in Appendix B.

Further discussion of noise analysis will occur in subsequent sections as appropriate.

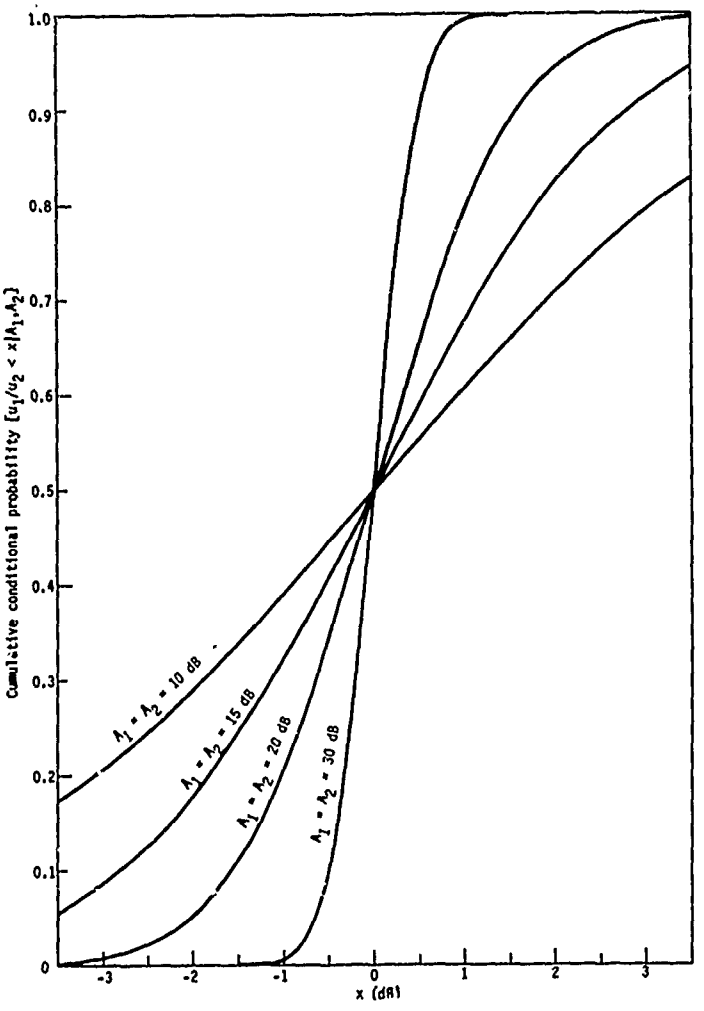

Fig. 4. Cumulative conditional probabilities of the quotient of two Rician variables; $\sigma_1 = \sigma_2 = 0$ dB.

Broadband Calibration Waveforms

There are two different forms of useful broadband calibration waveforms. One is a transient-type signal with a limited time duration. The second is a continuous deterministic broadband waveform, such as a pseudorandom waveform. Both waveforms have the same theoretical potential; however, each type has possible practical advantages. The practical advantages of the transient waveform are (1) the ability to recognize multipath interference directly from the temporal response without the use of correlation or transform methods, and (2) the possible use of

high-power transient sources such as explosive charges, air guns, and spark discharges as calibration signals. The practical advantage of the pseudorandom signal is the continuous transmission, which will allow a higher average power than conventional sources do and will provide better signal-to-noise ratios. It is believed that the information rate achievable with a pseudorandum source may be as much as an order of magnitude higher than that achievable with a transient source. Also, the two-state condition normally associated with pseudorandom sequences can alleviate problems with power amplifiers, since the projector can be driven by an appropriate switching configuration.

With transient waveforms, it is essential that the generated transient have a broad bandwidth and be practical from the standpoint of signal generation and repeatability. Although the impulse function has a desirable spectrum, it has been ruled out because of practical reasons. The two transient waveforms that have been investigated are a synchronous one-cycle pulse of a sinusoidal wave and a step function waveform. The spectrum of a step function has the well-known 1/f spectrum and is considered as a most appropriate calibration waveform. The energy spectrum of a synchronous one-cycle pulse of a sinusoidal wave is given by

$$E(f) = \left[\frac{\sin \pi(f/f_0)}{\pi f_0[1 - (f/f_0)^2]}\right]^2 . \tag{36}$$

The shape of the energy spectrum is shown in Fig. 5. Also shown plotted on the same figure is the curve for a 6-dB/octave boost applied to the

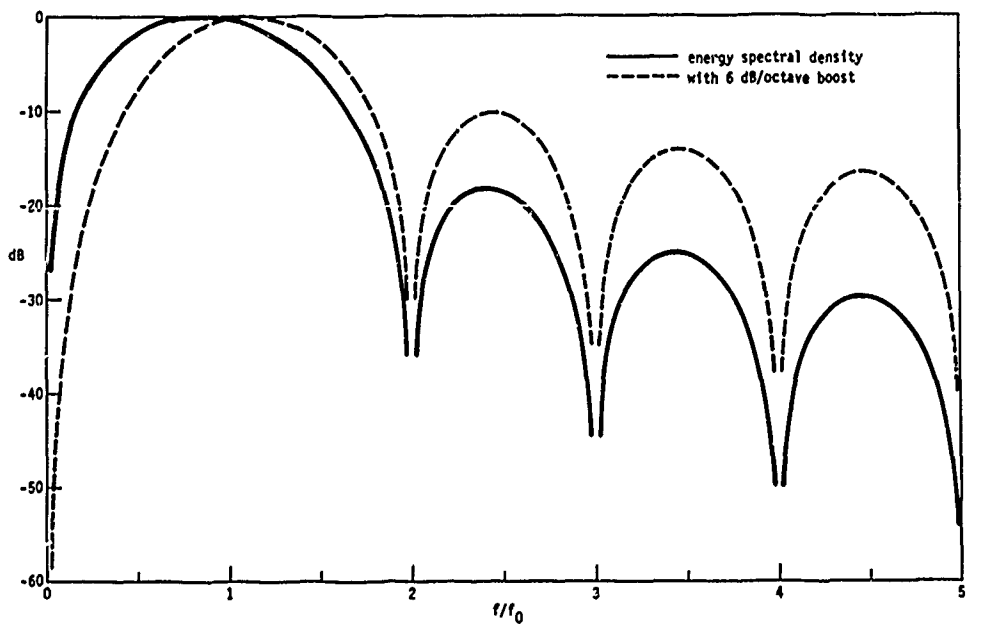

Fig. 5. Energy spectral density, one cycle of sine wave at frequency f_0.

spectrum of Eq. (36). In both cases, the spectra have been normalized to a zero-decibel level for the maximum spectral density. A universal curve is shown with the spectral density plotted as a function of f/f_0 with f_0 is the frequency associated with the one-cycle sinusoid. The spectrum with the 6-dB/octave boost is included because it is felt that this may be more indicative of the actual energy spectrum in the water. Note the zeroes that occur for $f/f_0 = 0, 2, 3$, etc. From the spectrum with the 6-dB/octave boost, considering only the portion between the first two zeroes, it is apparent that the useable frequency range will cover about 3 octaves.

One of the advantages stated for the transient waveform is the ability that it provides for recognizing multipath interference directly from the total system's temporal response. To realize this advantage, the response due to the direct arrival must be essentially zero when the first multipath signal arrives. Then, theoretically, the response may be truncated so as to retain only the signal due to the direct arrival. If the signal due to the direct arrival has truly gone to zero before truncation, the truncation will, of course, have no effect on the energy spectral density of the signal transform; however, there will be an effect on the contaminating noise. This result should be somewhat advantageous in that the total noise energy contribution in the transform will be decreased by the truncation, with expected signal-to-noise improvements. The energy spectral density of the truncated noise is given by

$$E_N^T(f) = T \int_{-\infty}^{\infty} P_n(f') \left[\frac{\sin \pi(f - f')T}{\pi(f - f')T} \right]^2 df'. \tag{37}$$

Equation (37) is derived by taking the convolution of the noise power spectral density and the Fourier transform of the autocorrelation function of the square truncating waveform. It should be clear from Eq. (37) that although the total noise energy is decreased according to the truncation width T, a discrete term in the noise spectra will tend to be smeared in the truncated spectrum because of the $(\sin x)/x$ convolution term. This fact is equally true for a d-c term in the noise where the amplitude spectra due to the d-c term will take the form

$$\left| E_{dc}^T(f) \right| = TE_0 \left| \frac{\sin \pi fT}{\pi fT} \right|, \tag{38}$$

where T is the truncation width and E_0 is the amplitude of the d-c component. Because the medium will not support a d-c term, it is clear that this d-c term should be removed before taking the Fourier transform. It can be removed by integrating over the truncated region of the response, averaging, and subtracting this average from each of the sampled values in the truncated region.

If part of the signal is eliminated in the truncation process, conceivably serious errors could occur in the estimation of the energy spectra, which would result in calibration errors, particularly if the effects are different in the standard being used and the unknown.

Another type of transient that has been considered is the step function. If the projector of Fig. 1 is connected through a switch to a battery, closing the switch will provide a step function of voltage to the projector. Opening the switch after the projector has stabilized will provide a negative step function of current. This waveform will not have the zeroes in the spectrum as produced by the single cycle of the sinusoidal wave; however, it could have zeroes in the spectrum produced by zeroes in the system response.

Disadvantages of transient inputs are the high ratio of peak-to-average signal and the small duty cycle normally imposed by the requirement that the system be allowed to stabilize completely before the next transient is applied. These properties can result in a serious dynamic range problem for the transient-type signal. This situation can be improved considerably by using a continuous pseudorandom waveform as the calibration signal. First, the peak-to-average signal will approximate that normally associated with a Gaussian waveform. Second, the duty cycle will be 100 percent. The waveform is deterministic and repeatable, so signal averaging can be used to discriminate against certain types of noise. Stabilization time does not pose a serious problem. As a matter of fact, the pseudorandom signal may be thought of as the pseudorandom combination of harmonically related sinusoids with a fundamental frequency equal to the inverse of the period of the pseudorandom sequence, where the phases of the sinusoids in the combination are such as to avoid extreme peaks. Some properties of pseudorandom sequences are described in Appendix C. From Appendix C, the power spectral density of the pseudorandom sequence is

$$P(f) = p[(\sin \pi fp)/\pi fp]^2, \tag{39}$$

where p is the period of the shift pulse, or $(2^n - 1)p$ is the period of the sequence. It is seen from Eq. (39) that by keeping f small so that $fp < 0.442$, the higher frequency components of the sequence are down only 3 dB from the maximum value. This means that all of the harmonically related sinusoids mentioned above are of approximately the same amplitude. The calibration processing, where multipath discrimination is not required, is exactly equivalent to that for the transient waveform. Where discrimination against multipath signals is desired, generation of either the autocorrelation functions of the receiver outputs or the cross-correlation functions of the system inputs and outputs is required. Truncation then is performed in the transform domain, provided that correlations due to direct and indirect signals are resolvable.

Description of Experiments

To gain insight into the problems involved in adapting the theories of broadband signals to practical underwater sound transducer calibration measurements, simplified comparison-type experiments have been performed at the NRL-USRD Leesburg open-water calibration facility. Basic interest in these first experiments was to determine something about the accuracy that could be obtained under well-controlled conditions and to better define associated problems. Such problems as hydrophone resonances, reflection interference, and ambient noise were minimized by the choice of acoustical instrumentation, frequencies, and rigging configuration. On the other hand, the frequency range 10 Hz to 1 kHz chosen for the experiments is in the range where reflection and noise problems usually predominate in open-water sites. In addition, considerable 60-Hz power line interference also was present in some of the output signals. Thus, these results cannot be interpreted in any way as having been obtained under idealized conditions.

The Leesburg Facility is located on a natural spring somewhat atypical of those found through Florida in that it is bowl-shaped rather than funnel-shaped. The spring is roughly elliptical, with major and minor axes of 50 and 40 m, respectively. The sidewalls of the cavity are composed of dolomite-type rock mixed with compacted organic material. The sides fall sharply to a mean depth of approximately 45 m. The well of the facility is located such that the hydrophone can be rigged roughly in the center of the cavity volume. An omnidirectional sound source was rigged at the same depth on the major axis at the distance 1 m from the hydrophone. This rigging configuration minimizes reflection problems, because reflections arriving at the hydrophone from walls of the cavity and the air-to-water interface tend to cancel each other. For the arrangement used, the travel time for these reflections is about 24 ms.

In addition to multipath interference, ambient noise of the site as well as the noise of the associated electronics further degrade the signal. Figure 6 shows a typical noise profile of ambient water noise associated with the site. At 20 Hz, this noise level corresponds to a voltage level of approximately -85 dB re 1 V at the output of the receiving system that was used, which is well below noise levels generally contributed by the electronics.

The hydrophones used in these experiments were chosen because their sensitivities are flat throughout the frequency range 1 Hz to 10 kHz. The hydrophones were the USRD types F36, F37, and F50, which are described by Groves [17] in a recent report. Their free-field voltage sensitivities, previously determined by conventional calibration, are listed in Table 1.

A USRD type J13 electrodynamic projector was used as the sound source. This projector was chosen because of its good low-frequency response and its ability to be driven intermittently with up to 2 A of current. The projector has a highly damped resonance at about 40 Hz. Characteristics of this projector also are described in the report [17] by Groves. A typical transmitting current response for the J13 is shown in Fig. 7.

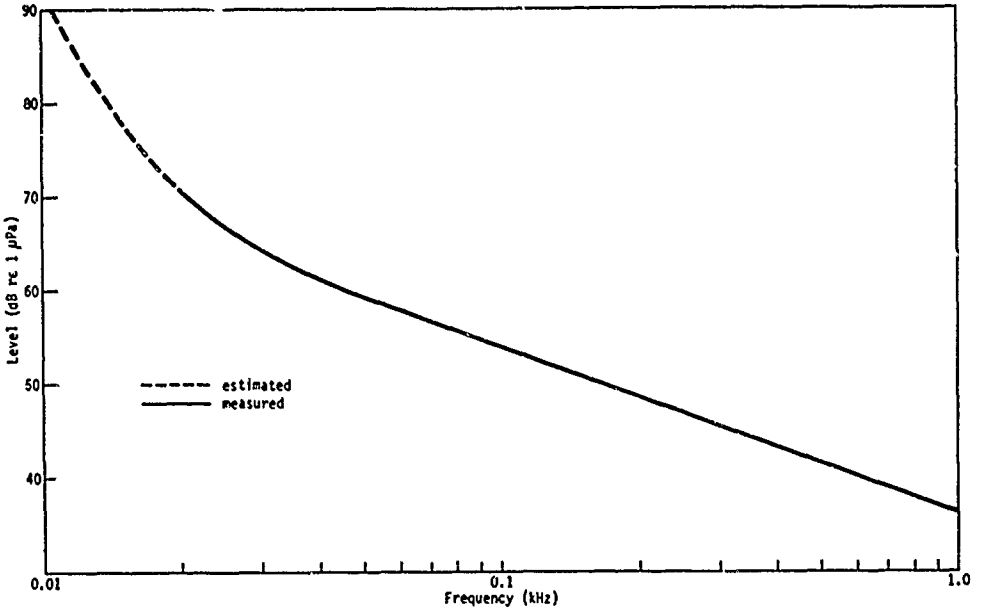

Fig. 6. Noise pressure level per hertz at the 12-m depth, Leesburg Facility (from unpublished data of Dr. J. E. Blue).

Table 1. Free-field voltage sensitivities of hydrophones used in broadband calibration experiments.

Hydrophone	Sensitivity (dB re 1 V/μPa)
F36	-202.3
F37	-204.7
F50	-206.0

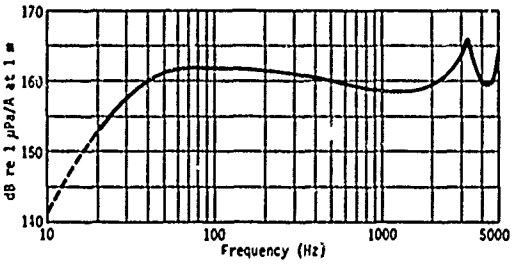

Fig. 7. Typical transmitting current response, USRD type J13 transducer.

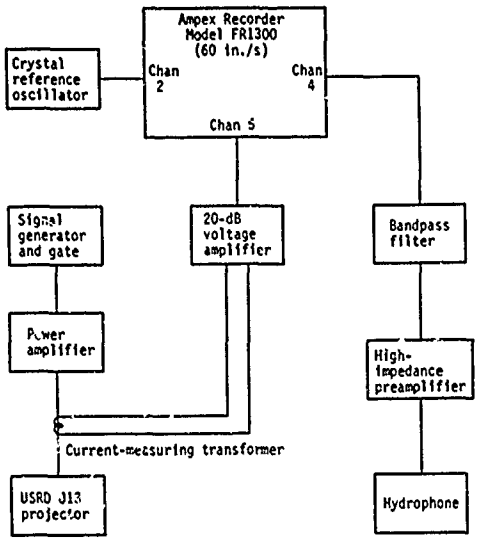

Fig. 8. Data-acquisition system.

Because a digital recorder was not available at the measurement site, it was necessary to record the data in analog form on an Ampex FR1300 magnetic tape recorder for later processing. All recordings were made at 60 in./s, using FM electronics. A block diagram of the data-acquisition system is shown in Fig. 8. The signal generator and gate provided a one-cycle pulse of the desired frequency to the power amplifier. The power amplifier, with appropriate impedance matching, was used to drive the J13 projector, which produced the acoustic signal in the water. The output of the current transformer used to measure the current into the J13 was amplified and recorded on one channel of the Ampex recorder. The recording level was adjusted so that the peak voltage was approximately 1 V. The output of the hydrophone in the acoustic field generated by the J13 was amplified, filtered, and recorded on a second channel of the Ampex recorder. A bandpass filter was used, but the principal concern was the low-pass characteristics; therefore, the upper frequency cutoff was set at from 1/3 to 1/2 of the sampling rate to be used in subsequent processing, to avoid possible aliasing effects. The filter's attenuation characteristics provided 48 dB/octave rejection in the attenuation band. The low-frequency cutoff was set at 3 Hz for all of the experiments. In addition, the output of a crystal-controlled oscillator was recorded on a third channel of the Ampex recorder. Because this channel was to be used to provide the sampling pulses for later data processing, the oscillator was set at a frequency equal to the proposed sampling rate.

For a given experiment, the one-cycle pulse was repeated 100 times and the required recordings were made. Temporal separation between the pulses was such that the entire system had reached its quiescent state before the next pulse was applied. This repetition of the experiment was performed in order that "signal averaging" could be used in the ultimate processing of the data. The experiment was conducted two different times in as near an identical manner as possible, using two

different hydrophones, both of known sensitivites. Gain controls remained constant throughout both experiments. One of the hydrophones was considered as the hydrophone to be calibrated; the second was considered as the calibration standard.

The data thus obtained were returned to the main laboratory at Orlando for processing by the PDP-8/I minicomputer. A block diagram of the data playback and digitizing system is shown in Fig. 9. Recorder playback speed was 7.5 in./s, or one fourth of the recording speed, to allow for interfacing with the analog-to-digital converter and multiplexer of the PDP-8/I minicomputer. Thus, actual frequency values on playback filters were divided by 4 to correspond to the same frequency in the recording time frame. To avoid confusion, however, time and frequency will always be considered to be in the recording time frame in this report, unless otherwise specified.

On tape playback, the sampling pulses for the data channels were obtained by a hard-limiting of the reference frequency that was recorded for this purpose. Sampling pulses were generated from this hard-limited signal. Sampling rates (in recording time) were 1024, 2048, or 4096 samples per second, depending on the frequency range to be covered. The J13 current signals and the hydrophone voltage response signals were sampled and stored in the PDP-8/I core memory. Storage in core memory was initiated by thresholding the current signal. A small part of the core memory was used as a rotating buffer store so as to preserve samples of the time series immediately preceding the signal.

Additional antialiasing filtering was provided on playback for the voltage response signals. Core storage was limited in the PDP-8/I to 2048 11-bit-plus-sign binary words, thus the maximum storage was 2 s of data at the lowest sampling rate. The 11-bit words correspond to a total dynamic range of 66 dB. Levels were adjusted before beginning the digitizing process to make full use of this dynamic range.

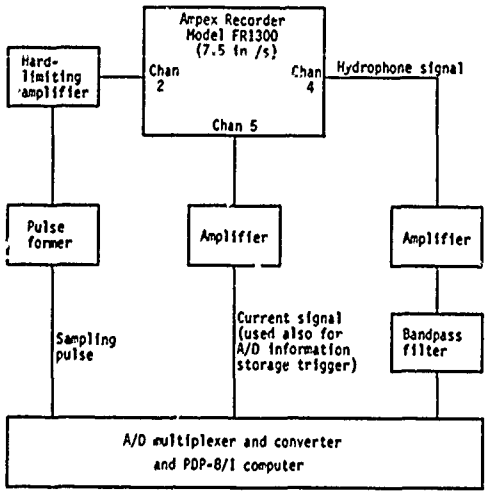

Fig. 9. Data playback and digitizing system.

After each transient current waveform and voltage response waveform was digitized, the digital data were transferred to DEC magnetic tape (used by the PDP-8/I for bulk storage) and the analog-to-digital converter and multiplexer were made ready to receive the next set of transient waveforms. Data were stored in blocks of 128 words each, with 8 blocks or 1024 words usually used to characterize a waveform. When all of the data for a given experiment had been digitized, there existed in digital form 100 sets of transient current waveforms and voltage response waveforms for both the hydrophone being calibrated and the hydrophone being used as the standard.

The next step in the processing was to recall each member of a set back into core and generate an ensemble average for that set. Because signals added coherently in the generation of these averages, discrimination against the normal types of noise encountered was achieved. It should be pointed out that signals were not completely coherent, because errors in time displacement of ±1/2 sample periods were possible in the digitizing of each transient waveform; however, sampling rates were sufficiently high so that this type of error was considered negligible. After each of the 4 transient averages was generated, it was transferred back to DEC tape storage.

The next step was to recall each of the averaged transient waveforms into core memory and generate the discrete Fourier transform (DFT) by use of one of the fast Fourier transform (FFT) algorithms. The energy amplitude spectrum then was generated by appropriate combination of the real and imaginary parts of the transforms. This spectrum was converted to a decibel scale and transferred back to the DEC tape storage. This transfer was made for each of the four transient waveforms. The four transforms then were recalled into core memory and combined according to Eq. (13) to provide a calibration of the hydrophone considered the unknown with respect to the hydrophone being used as a standard. No smoothing was applied either in the spectral estimates or the final calibration calculations.

In digitizing the transient waveforms, the last four blocks of data represented a very good measure of the noise of the systems. The DFT's of these noise blocks were taken to give an estimate of the energy spectrum of the noise.

Results and Conclusions

Figure 10 shows computer plots of the first 0.5 s of the J13 current waveform where the input was a one-cycle pulse of a 65-Hz signal. A typical sample of the raw current waveform is shown as well as one of the two averaged J13 current waveforms. Note that very little noise is associated with the raw current waveform. Figure 11 shows the same sort of computer plots for the F37 voltage response waveforms during the same experiment. Note the noise in the raw waveform and the general effectiveness of the signal averaging in discriminating against that noise.

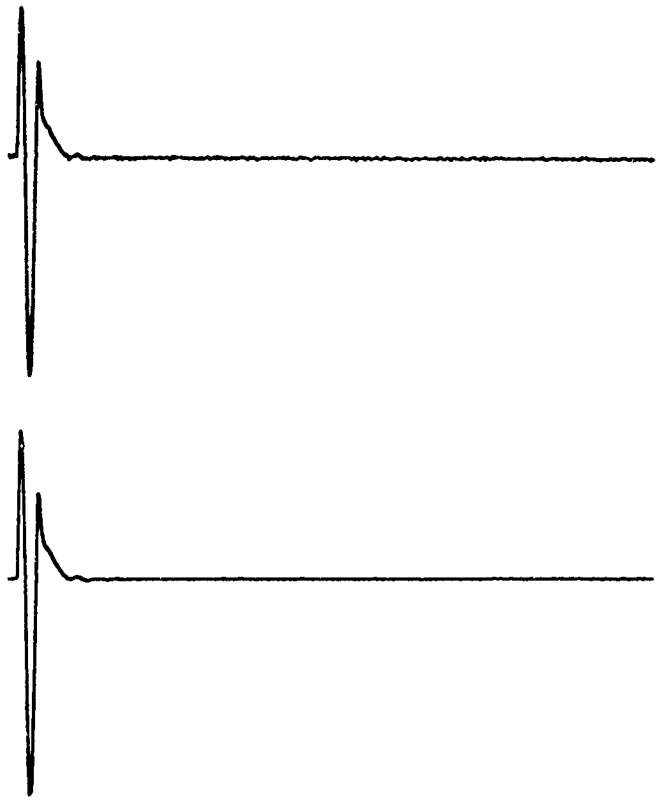

Fig. 10. J13 current waveforms, one cycle, 65-Hz signal. Top: raw J13 current waveform; duration, 0.5 s. Bottom: averaged J13 current waveform (100 waveforms used in average); duration, 0.5 s.

Figure 12 shows the same kind of computer plots for the F50 voltage response waveforms during the same experiment with the one-cycle 65-Hz pulse. Note the high level of 60 Hz in the raw waveform; this was typical of data taken with both the F50 and F36 hydrophones. The averaged waveform again shows the extreme effectiveness of the signal averaging. Conclusions from Figs. 10-12 are that considerably fewer signals could have been used in the signal averaging, thus reducing the total time for data acquisition.

Figure 13 shows the relative energy spectra for the averaged J13 current waveform, the F50 averaged voltage response waveform, and the F37 averaged voltage response waveform for the experiment using the one-cycle pulse at 65 Hz. The levels indicated are relative, but the F50 and F37 spectra are on the same relative scale. These spectra compare favorably with the calculated spectra as shown in Fig. 5. The lack of depth in the expected null at 130 Hz probably is due to nonlinearity of the J13 projector. Certainly, the shallowness of the nulls cannot be

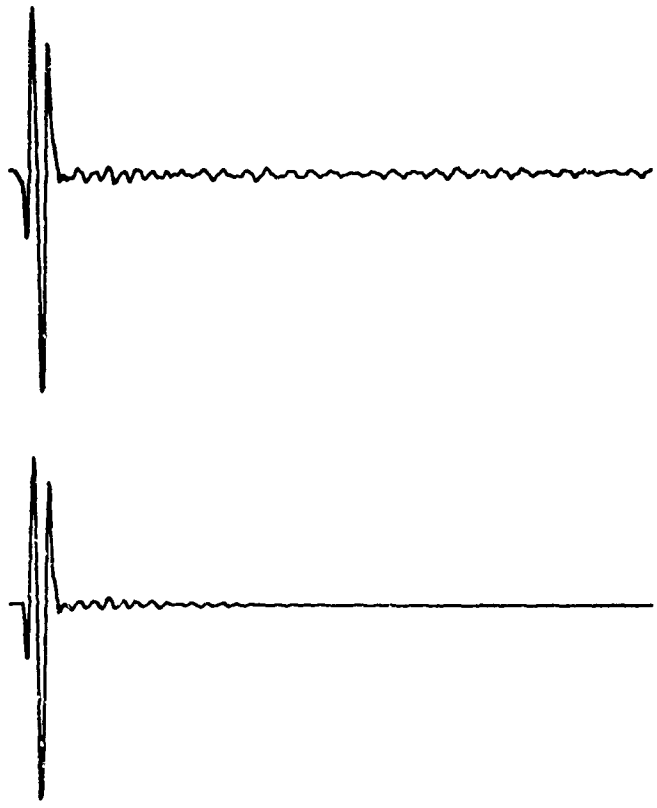

Fig. 11. F37 response waveforms, one cycle, 65-Hz signal. Top: raw F37 response waveform; duration, 0.5 s. Bottom: averaged F37 response waveform (100 waveforms used in average); duration, 0.5 s.

attributable to noise alone. No spectral smoothing has been applied to any of the spectra calculated. Although the variations of the voltage response spectra for frequencies below 10 Hz are unusually large, the hypothesis that they are due to noise alone cannot be rejected. Only one of the calculated current spectra is shown, because of their similarity.

Figure 14 shows calculated noise spectra for the J13 current measurements and the two voltage response measurements for the 65-Hz data. These spectra were computed from the last four data blocks of the appropriate average, where effects due to the signal were assumed to be negligible. Relative scales for these noise spectra are the same as those for the energy spectra with which they are associated. Both the averaged noise spectra for the F37 and the J13 appear to be close to that attributable to tape recorder noise and/or quantization noise. The noise spectrum for the F50 shows peaks at 60 Hz and approximately 7 Hz that are 25-30 dB higher than the noise of the F37. This feature is undoubtedly one of the causes of the low-frequency fluctuations in the energy spectral density of the F37.

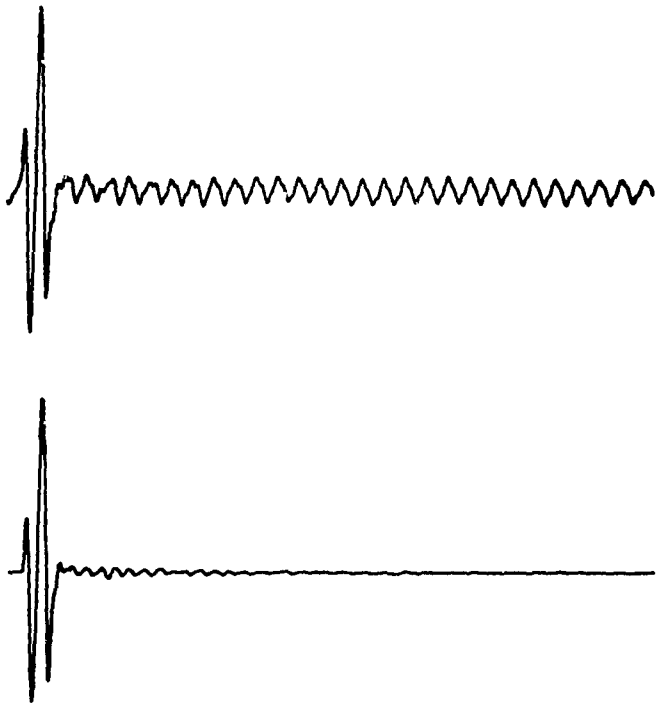

Fig. 12. F50 response waveforms, one cycle, 65-Hz signal. Top: raw F50 response waveform; duration, 0.5 s. Bottom: averaged F50 response waveform (100 waveforms used in average); duration, 0.5 s.

Figure 15 is a computer plot of the calibration of the F37 in which the F50 is used as the calibration standard for the 65-Hz experiment. The results compare most favorably with the known sensitivity of the F37 (-204.7 dB re 1 V/μPa), particularly since no spectral smoothing or smoothing of the final calibration was used. Even the grossest smoothing would provide a calibration accuracy of ±0.5 dB from 120 Hz down to almost 10 Hz, which is much better than was expected. There is an apparent rise in sensitivity at the lower frequency of approximately 1 dB, which is completely anomalous. This rise does not seem attributable to the noise, because the higher noise level of the F50 at the lower frequencies should have caused a droop in sensitivity at the lower frequancies rather than a rise. It has been postulated that this anomalous behavior may in some way be due to the different capacitances of the F37 and F50 and some unknown loading effects on the transducer outputs. These effects would cause a rise in the measured sensitivity at the lower frequencies for the F37. This explanation is not really considered a satisfactory one, however. The flat part of the sensitivity curve between 50 and 120 Hz is 0.3-0.4 dB lower than the -204.7 dB value that had been measured for the F37; however, this result could very easily be due to errors in the original calibrations of the F37 and/or the F50 transducers.

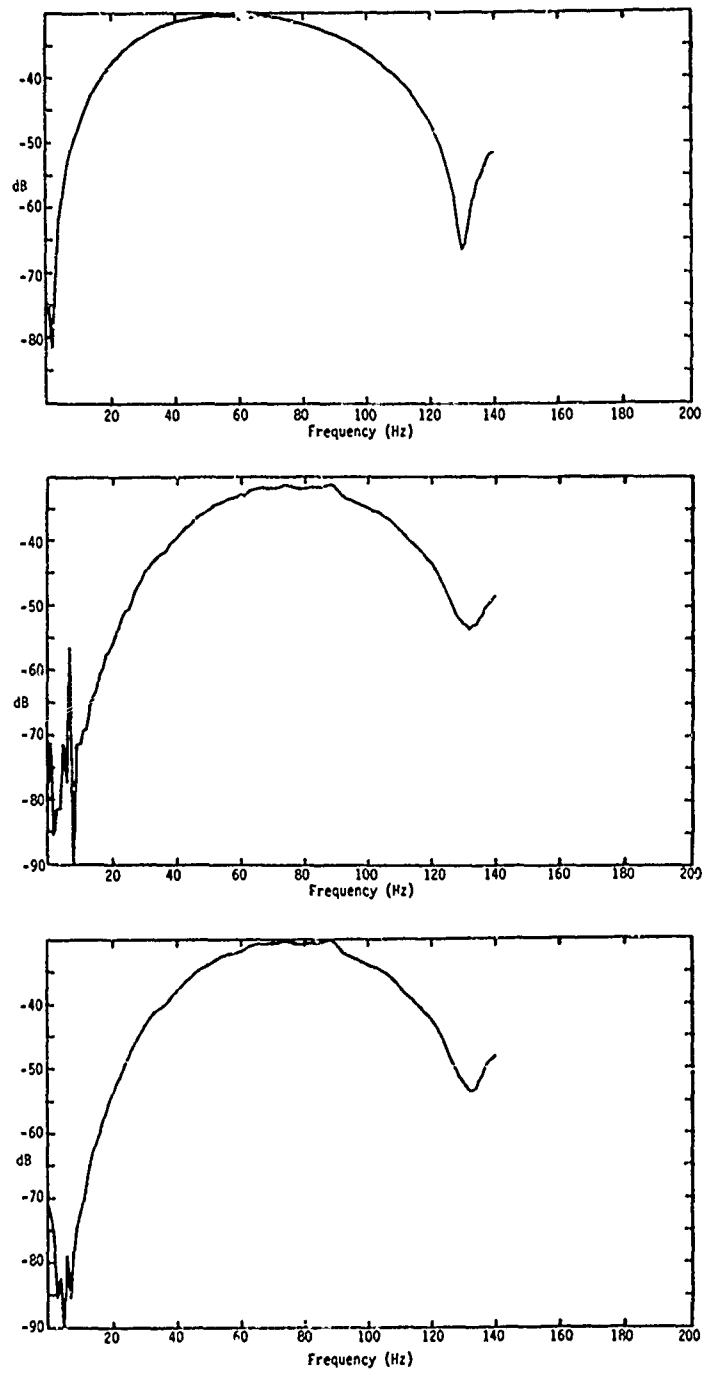

Fig. 13. Energy spectra obtained in calibration experiments using one cycle of 65-Hz signal. Top: relative spectrum, J13 current. Middle: relative spectrum, F50 response. Bottom: relative spectrum, F37 response.

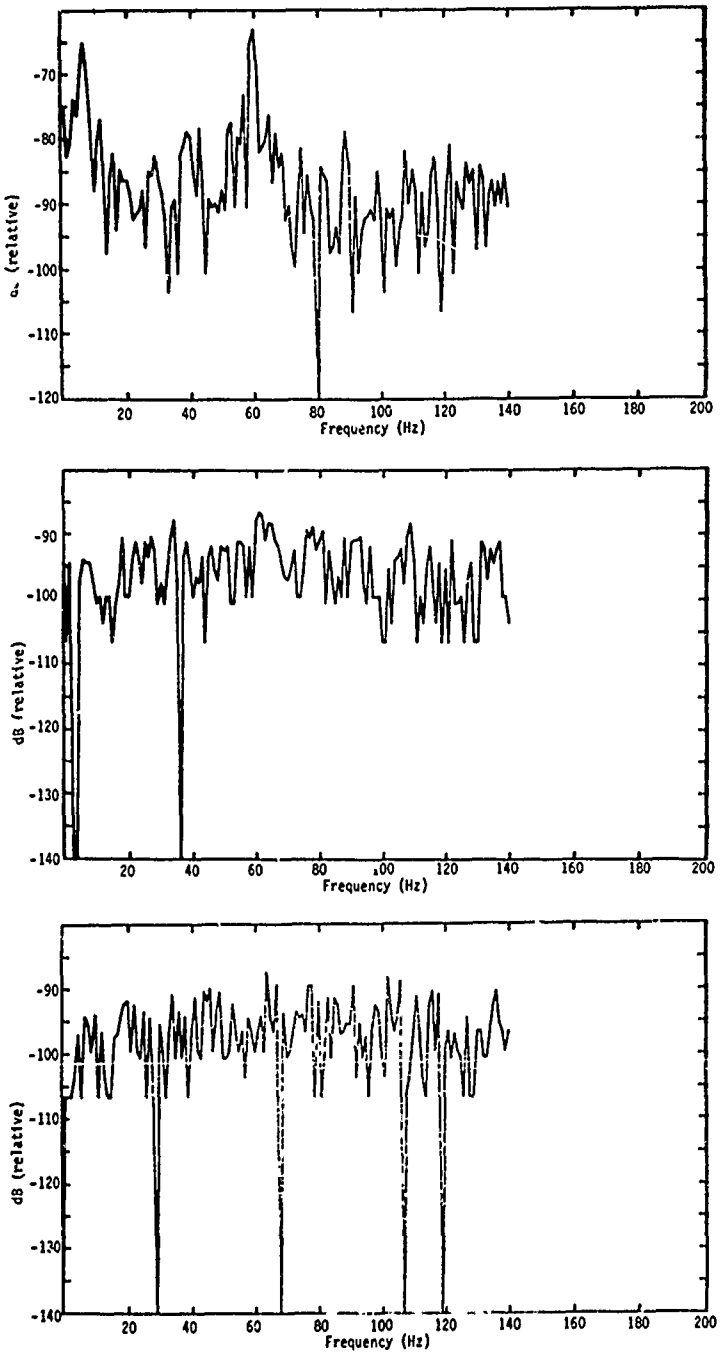

Fig. 14. Noise power spectra (taken from 65-Hz pulse data). Top: F50 noise spectrum. Middle: F37 noise spectrum. Bottom: J13 current noise spectrum.

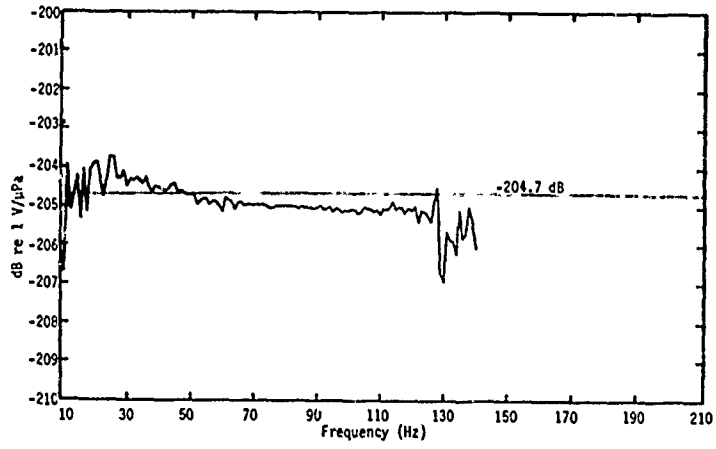

Fig. 15. F37 receiving response obtained by broadband methods with the F50 as the standard (one cycle of 65-Hz signal).

Figure 16 shows the effects of truncation of the original transient waveforms on the calibration results. In all cases, the transient waveform averages were zeroed before truncation rather than after. There seems to be little effect due to truncation of the waveforms, except for changes in the fluctuations at frequencies below approximately 25 Hz. Two inferences that may be drawn from the similarity between the curves are (1) acquisition of 0.25 s of data would have been adequate for this experiment and (2) apparently there are no real noise problems, except possibly for frequencies below 25 Hz.

Figures 17 and 18 show a summary of the results of calibration experiments using a one-cycle 30-Hz pulse to drive the J13 projector. Computer plots of the estimated current spectrum and the voltage response spectra are shown in Fig. 17. In this case the F36 transducer was used as the calibration standard and the F37 was used as the transducer to be calibrated. The calculated spectra agree with what was generally expected, except for a small irregularity in the spectra of both the F36 and F37 at approximately 6 Hz. The fact that the irregularity occurred in both spectra strongly indicates that it is real and probably due to an anomalous behavior of the J13 projector or to a possible resonance in the rigging.

Figure 18 shows the calculated calibration curve. The results are considered fantastically good, particularly in view of the fact that no smoothing has been used. Not only are the results good from 10 Hz to just below the 60-Hz null frequency of the spectra, but they are also considered to be excellent between the spectrum nulls at 60 and 90 Hz. There is also evidence that the calibration is good even beyond the 90-Hz frequency that represents the third harmonic null in the spectrum.

Figures 19 and 20 show a summary of the results of calibration experiments using a one-cycle 50-Hz pulse to drive the J13 projector. Again the hydrophones used were the F36 and F37. The same irregularity

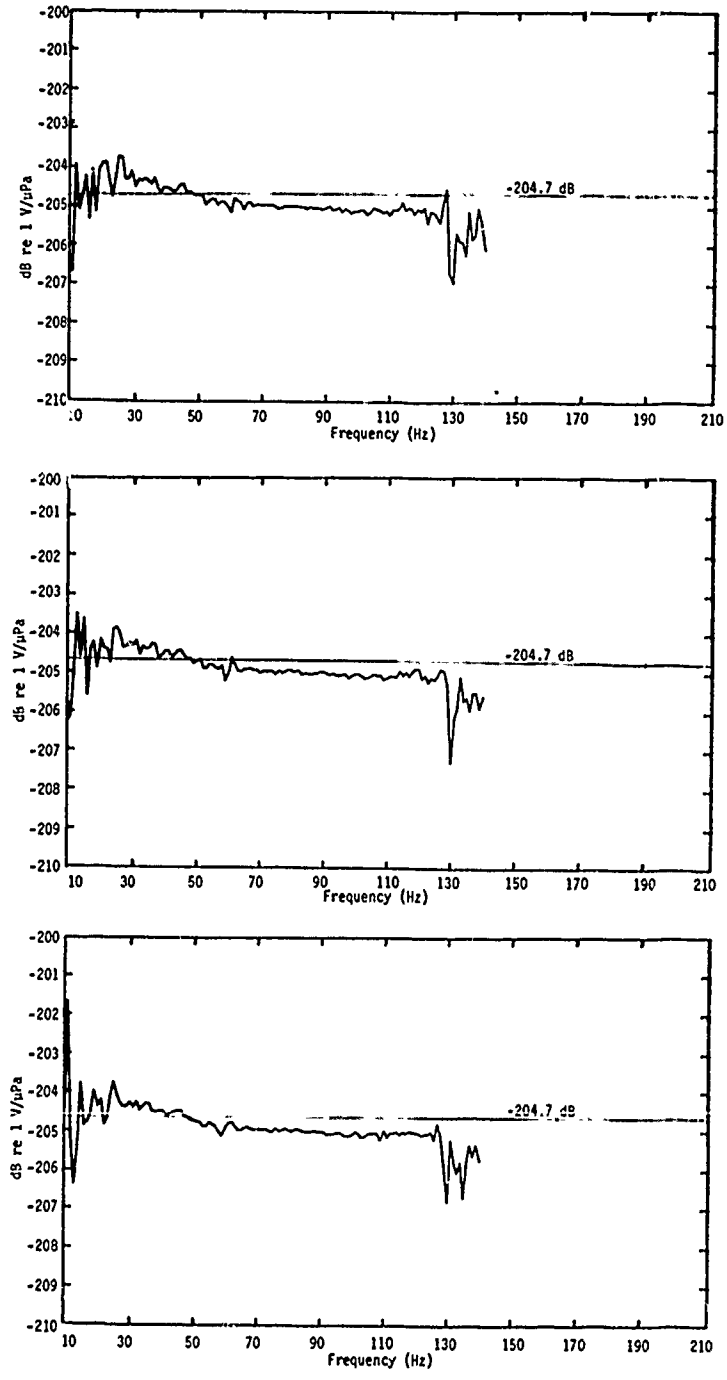

Fig. 16. Effects of truncation on calibration results. Curves are F37 response obtained by using the F50 as a standard with one cycle of 65 Hz as the calibration signal. Top: calibration based on full 1 s of data. Middle: average waveforms truncated after 0.5 s. Bottom: average waveforms truncated after 0.25 s.

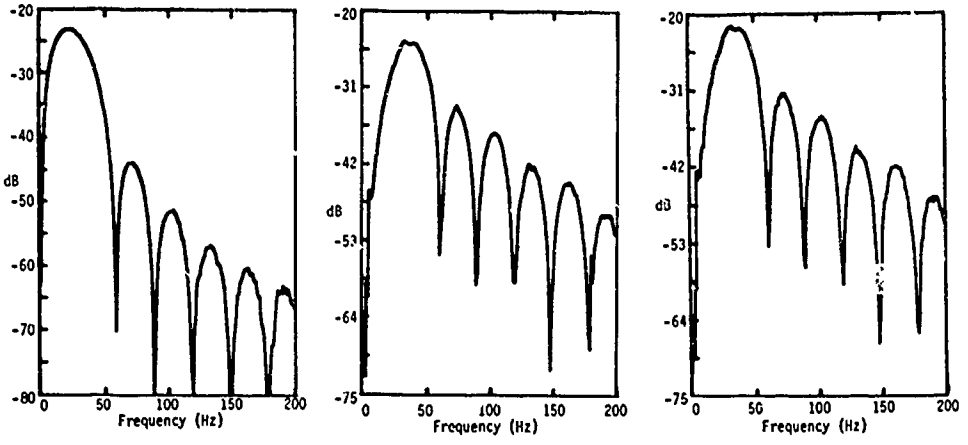

Fig. 17. Energy spectra obtained in calibration experiments with one cycle of 30-Hz signal. Left: relative spectrum, J13 current. Middle: relative spectrum, F36 response. Right: relative spectrum, F37 response.

at approximately 6 Hz that occurred in both the F36 and F37 spectra in the 30-Hz experiment occurred in the spectrum of the F36 in the 50-Hz experiment; however, it did not occur (at least not to the same extent) in the F37 spectrum. A possible inference from this is that operating the J13 at the level being used, at which it is known to be nonlinear, is exciting some unknown resonance in a more or less unstable manner. Figure 20 shows the computer plot of the calculated F37 calibration, with the F36 regarded as the standard. Again, the results are exceedingly good.

Figures 21 and 22 show the summary of results where a one-cycle pulse of 1 kHz was used as the calibration signal. The F36 and F37 transducers were used in this experiment. Figure 21 shows the energy spectra of the J13 current response and the two voltage responses. As was expected, this experiment demonstrated more than any other the need for spectral smoothing. The need was brought about by the relatively

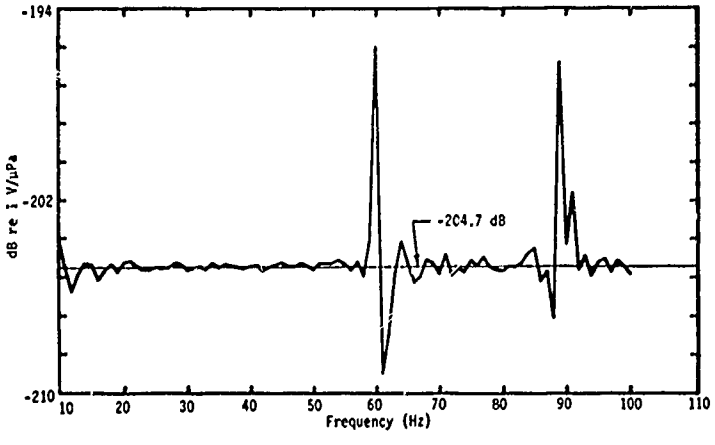

Fig. 18. F37 receiving response obtained by broadband methods with the F36 as the standard (one cycle of 30-Hz signal).

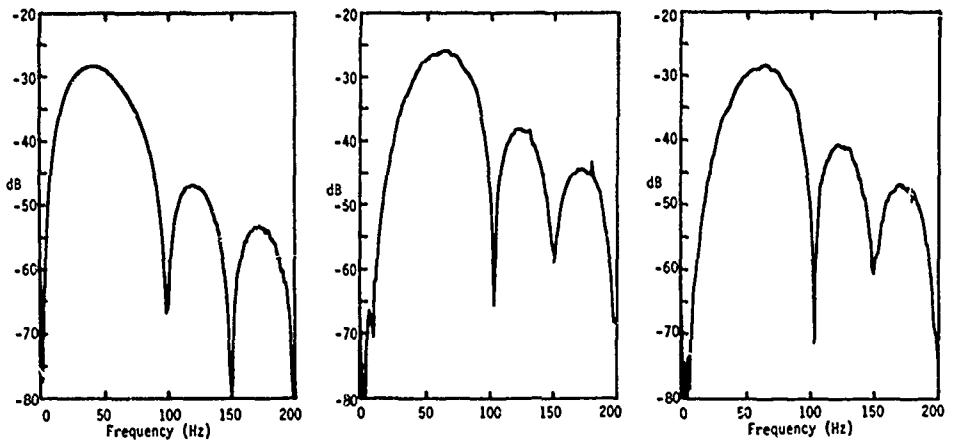

Fig. 19. Energy spectra obtained in calibration experiments with one cycle of 50-Hz signal. Left: relative spectrum, J13 current. Middle: relative spectrum, F36 response. Right: relative spectrum, F37 response.

short duty cycle of the 1-ms transient plus the reduced response of the J13 to higher frequency voltage inputs. Figure 22 shows the calculated calibration response of the F37 with reference to the F36 as a standard. As was expected, there was more noise than usual in the calibration curve. Nevertheless, the results were considered good.

In addition to this series of experiments using a single-cycle sinusoid as a calibration signal, experiments using step function inputs were also performed. Because of chatter in the manual switch that was used to generate the step function, however, these data were discarded.

Another procedure not fully exploited but of some consequence was discrimination against periodic noise waveforms by an appropriate shifting in time of a signal-free portion of the time series and subtracting it from the signal. This procedure is particularly applicable to discrimination against 60-Hz noise and its harmonics brought about by an

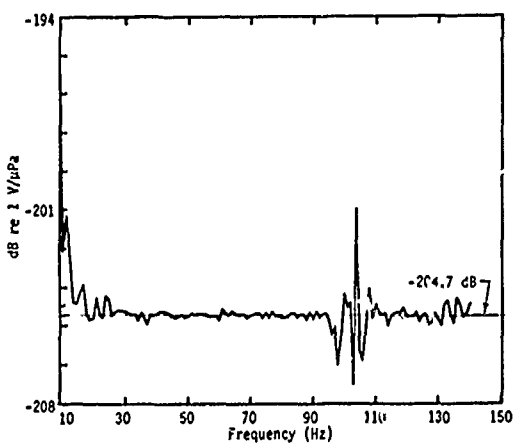

Fig. 20. F37 receiving response obtained by broadband methods with the F36 as the standard (one cycle of 50-Hz signal).

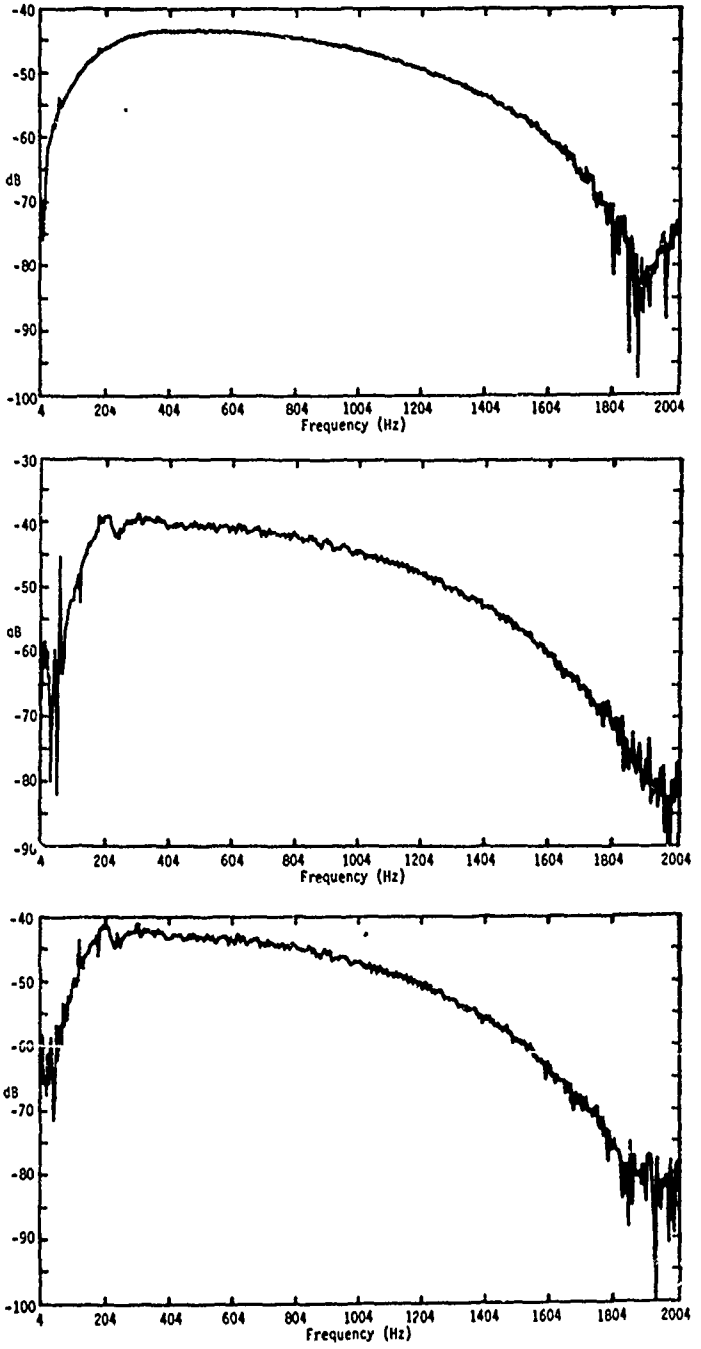

Fig. 21. Energy spectra obtained in calibration experiments with one cycle of 1-kHz signal. Top: relative spectrum, J13 current. Middle: relative spectrum, F36 response. Bottom: relative spectrum, F37 response.

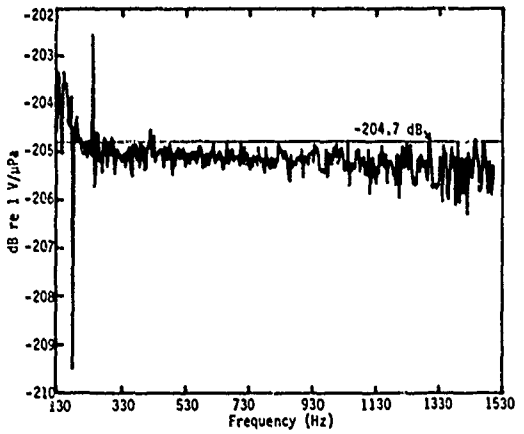

Fig. 22. F37 receiving response obtained by broadband methods with the F36 as the standard (one cycle of 1-kHz signal).

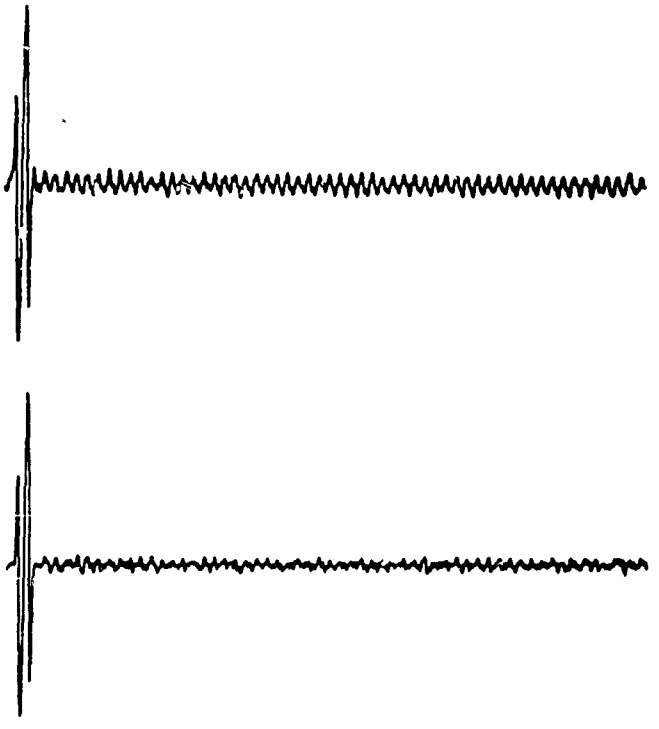

Fig. 23. Removal of periodic noise from transient signal waveform. Top: raw waveform that includes periodic noise. Bottom: same waveform as top curve but with periodic noise removed by shifting signal-free portion back an integral number of periods and subtracting.

inadequate grounding system. An example is shown in Fig. 23. Results in preliminary experiments using this technique have been very good. The technique is of some importance because many transducers requiring calibration may have been designed so that adequate grounding is not possible. Effort in this area has been limited and should be expanded in future work.

The general conclusions from the entire series of rather simplfied experiments was that feasibility of the general method was definitely established. As a matter of fact, it was felt that the accuracy of the results within the useable frequency ranges was better than usually is achieved with the present conventional operational systems.

Future Work

The primary objective of future work in this on-going effort will be to define the exploratory development of an operational underwater acoustic calibration system based on broadband calibration signals. The past effort has established the general feasibility of broadband methods, but the design of the experiments was compromised to carry out the early experiments most expeditously. The compromise involved a long and circuitous effort both in data acquisition and data reduction that would not be typical of an actual operational system. Future experiments will incorporate direct analog-to-digital conversion in the data acquisition and real-time signal averaging. In addition, several other areas of investigation have not as yet received adequate attention.

One such area of investigation that was originally planned but not carried out is a combined effort involving complementing theoretical analyses and computer simulation of broadband calibration experiments. This effort is a part of the future plans. The principal purposes of this investigation will be:

1. To understand more fully the effects of noise and how to treat it. The study will include quantization noise and noise due to finite sample sizes. It will also include a more complete study of the discrimination against periodic noise introduced by inadequate grounding such as has been briefly described.

2. To understand more fully truncation in the time domain of both signals and noise, and the general effectiveness of such truncation in the discrimination against multipath interference. The effort should apply also to truncation of cross-correlation and/or autocorrelation functions when broadband continuous waveforms are used.

3. To understand more fully the problems associated with spectral smoothing and/or smoothing of the final calibration curves. This smoothing is aimed primarily at obtaining best estimates in the presence of noise and includes conventional spectral smoothing such as Hann, Hamming, or Parzen windows, but is not limited to these types of smoothing.

Only one type of calibration waveform has been used in the initial experiments and that is the one-cycle pulse of a sinusoid. Even in

these experiments, the original digitized data were not saved so repeatability and statistical significance of variations could not be checked by data partitioning. Data partitioning in this context means the partitioning of a single experiment consisting of 100 sets of each transient waveform into four different experiments consisting of 25 sets of the current and voltage response transients. This sort of testing should be performed in future work. Just as important, however, is to obtain data using a step function input as the calibration signal. Still more important is to obtain and reduce data in which broadband continuous calibration signals are used.

The principal advantage of the broadband continuous waveform is that it will provide a smaller peak-to-average ratio than occurs with transients, which would greatly improve the utilization of the over-all dynamic range of the system and thus provide improved signal-to-noise ratios and higher information rates. Probably the easiest way to produce a broadband continuous waveform with the necessary deterministic properties is the use of pseudorandom noise (PN) waveforms. Some of the properties of PN sequences are derived and presented in Appendix C. The PN sequences are periodic and therefore readily lend themselves to signal-averaging techniques. One way in which the PN sequence may be thought of is as the combination of harmonic sinusoids with a fundamental frequency equal to the inverse of the period of the sequence, where the amplitudes of the harmonics are approximately the same over the frequency band to be used and the phases are such as to avoid the large peaks normally associated with a transient. In this context, the calibration may be viewed as a steady-state calibration in which the system is allowed to stabilize simultaneously for the entire harmonic set in contrast to stabilizing for one frequency at a time as in a conventional sweep-frequency calibration.

Another way of viewing the PN sequence is as a sequence of positive and negative step functions spaced in a pseudorandom fashion. A step function is considered as a most attractive transient-type signal in terms of realization and information rate criteria; thus, it follows that a PN sequence should be extremely good from an information rate standpoint.

One other point worth mentioning in regard to a PN sequence is its availability in a two-state condition. This fact may make power amplification simpler in that the projector may be driven directly from a d-c source, such as a battery, by an appropriate switching arrangement, with the switching between two allowable voltage (or current) states controlled by the PN sequence.

The initial experiments envisioned for PN sequences are much the same as those that have been used for the one-cycle sinusoid transients. The difference is that an attempt will be made to provide direct analog-to-digital conversion and real-time signal averaging.

Another consideration that should be given to planned experiments with PN sequences is the use of correlation techniques in the calculation of calibration results, particularly for cross-correlation techniques

where the PN input waveform (rather than the current) is cross-correlated with the output voltage response. This technique is especially attractive because the two-state voltage levels of the PN sequence will allow the correlation process to be reduced to a simple averaging process with appropriate sign changes.

Other investigatory areas that need to be covered prior to the definition of the exploratory development effort of the operational system are:

1. Analytical and experimental investigation of broadband calibration of transducers when resonances are involved.

2. Experimental investigations using broadband techniques in reciprocity calibrations.

3. Analytical and experimental investigations using broadband techniques to measure the complex response of transducers.

4. Cost-effectiveness trade-off studies of broadband calibration techniques versus conventional techniques.

The fourth item is of extreme importance as related to decisions to pursue the exploratory development. It should include a comparison of the time required for calibration by the two methods as well as a comparison of the accuracies. Perhaps the single criterion that would be of most use in the comparisons is the information rate associated with each of the two methods. The cost-effectiveness study also should assess the value of the measurement of complex responses, which is more easily associated with broadband techniques than with conventional techniques. It should include, further, the potential value of a system using broadband techniques to future research in such areas as the development of transducer equivalent circuits and the possible improvement in the characterization of nonlinear effects in transducers. Above all, it should weigh the cost and effort of developing a new type of system against the perceived value of the system. Preliminary judgements in favor of developing such a new system have already been made; however, these judgements should be verified and documented by the planned study prior to the final decision to proceed with exploratory development.

It is evident that work still to be performed before initiating an exploratory development phase is a major effort. In addition, there are important research efforts that should be continued even after the exploratory phase is started. The most important of these efforts are:

1. Study the use of adaptive techniques with broadband methods to increase discrimination against multipath interference associated with limited calibration enclosures and thus to increase low-frequency calibration capabilities in open-water facilities.

2. Study the potential of broadband methods for providing more accurate and sophisticated equivalent circuits for existing transducers.

Both of these efforts may very well involve the use of Laplace transform methods instead of the Fourier methods.

References

[1] G. E. Stedman, "Green's Functions," Contemporary Physics 9, 46-69 (1968).

[2] S. Goldman, *Transformation Calculus and Electrical Transients* (Prentice-Hall, Inc., New York, 1949).

[3] M. F. M. Osborne and J. L. Carter, "Transient Analysis of Linear Systems, Using Underwater Explosion Waves," J. Appl. Phys. 17, 871-873 (1946).

[4] P. Hohmann and M. M. Louden, "Bestimmung von Frequenzgängen elektroakustischer und elektromechanischer Wandler durch Einzelimpulse," Acustica 29, 40-46 (1973).

[5] Y. W. Lee, *Statistical Theory of Communications* (John Wiley & Sons, New York, 1960).

[6] W. B. Davenport, Jr. and W. L. Root, *An Introduction to the Theory of Random Signals and Noise* (McGraw-Hill Book Co., Inc., New York, 1958).

[7] E. A. Guillemin, *The Mathematics of Circuit Analysis* (John Wiley & Sons, New York, 1949).

[8] G. M. Jenkins and D. G. Watts, *Spectral Analysis and Its Applications* (Holden-Day, San Francisco, 1969).

[9] A. D. Whalen, *Detection of Signals in Noise* (Academic Press, New York, 1971).

[10] C. W. Horton, Sr., *Signal Processing of Underwater Acoustic Waves* (U. S. Government Printing Office, Washington, 1969).

[11] J. S. Bendat and A. G. Piersol, *Measurement and Analysis of Random Noise* (John Wiley & Sons, New York, 1966).

[12] L. D. Enochson and R. K. Otnes, *Programming and Analysis for Digital Time Series Data* (The Shock and Vibration Center, U. S. Department of Defense, Washington, 1968).

[13] R. J. Bobber, *Underwater Electroacoustic Measurements* (U. S. Government Printing Office, Washington, 1970).

[14] R. J. Bobber, "A General Reciprocity Parameter," J. Acoust. Soc. Am. 39, 680-687 (1966).

[15] L. L. Beranek, *Acoustic Measurements* (John Wiley & Sons, New York, 1949).

[16] A. Gray and G. B. Matthews, *A Treatise on Bessel Functions and Their Applications to Physics* (Dover Publications, Inc., New York, 1966).

[17] I. D. Groves, Jr., "Twenty Years of Underwater Electroacoustic Standards," NRL Report 7735, Feb 1974 (AD-776 214).

Appendix A

DERIVATION OF
A COMPLEX SPHERICAL RECIPROCITY PARAMETER

Normally, an acoustical reciprocity calibration involving spherical waves produces transmitting and receiving responses in terms of only the amplitudes of the quantities involved. If a response obtained in complex form by reciprocity methods is desired, the spherical reciprocity parameter must be expressed in complex form. Beranek gives such an expression [15]; however, a different derivation is given in this Appendix because the Fourier transform techniques used in it are in consonance with the theme of this report.

The original contact with the principle of reciprocity for most scientists and engineers usually has been its application to an electrical network composed of passive linear bilateral elements. The reciprocity principle is developed from the symmetrical form of the matrix that relates the dependent and independent variables. In such an n-port network, it can be shown that the short-circuit current at the i-th port produced by a voltage applied to the j-th port is the same as the short-circuit current produced at the j-th port by the same voltage applied to the i-th port.

In deriving the acoustical reciprocity parameter, it is customary to start with an electromechanical analog of a two-port electrical network where the force applied is the analog of the voltage and the velocity is the analog of the current. For the purpose of this derivation, the pressure applied to the acoustic radiating surface of the transducer will be considered as the voltage analog and the volume velocity of the radiating surface will be considered as the current analog. The two-port electromechanical circuit is shown in Fig. A1. Two simultaneous differential equations describe this circuit. If the Fourier transforms of these equations are taken, the result is

$$E(f) = Z_{11}(f)I(f) + Z_{12}(f)Q(f)$$

$$P(f) = Z_{21}(f)I(f) + Z_{22}(f)Q(f). \qquad \text{(A1)}$$

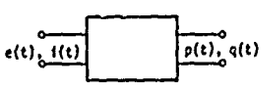

Fig. A1. Two-port electromechanical circuit; e(t) is the voltage at the electrical port, i(t) is the current at the electrical port; p(t) is the pressure at the mechanical port, and q(t) is the volume velocity of the radiating surface.

The reciprocity principle depends upon the relation $Z_{12}(f) = \pm Z_{21}(f)$, where a single consistent set of units is assumed. There is no reason why absolute values have to be used, inasmuch as the sign is dependent only on whether the transduction is electromagnetic or electrostatic. A positive sign will be assumed for this derivation. If the open-circuit voltage [I(f) = 0] at the electrical port is determined for an applied volume velocity at the mechanical port, and if the pressure with a blocked radiating surface [Q(f) = 0] at the mechanical port is determined for an applied current at the electrical port, then, by virtue of the equality of $Z_{12}(f)$ and $Z_{21}(f)$,

$$\left.\frac{E(f)}{Q(f)}\right|_{\text{open-circuit}} = \left.\frac{P(f)}{I(f)}\right|_{\text{blocked}}. \tag{A2}$$

The radiating surface of the mechanical port will produce an acoustic signal in the medium. If the medium is such that it will support only irrotational acoustic waves, then the acoustic field may be characterized by a velocity potential ϕ that will satisfy the wave equation

$$\nabla^2\phi = (1/c^2)\ddot{\phi}. \tag{A3}$$

If complete spherical symmetry is assumed, then the solution to Eq. (A3) for an outgoing spherical wave is given by

$$\phi(r,t) = (1/r)f(t - r/c), \tag{A4}$$

where f(t) is an arbitrary but well-behaved function and c is the sound speed in the medium. Now the pressure in the medium and the particle velocity are given by

$$p = -\rho_0\dot{\phi}$$

$$v = \nabla\phi, \tag{A5}$$

where ρ_0 is the density of the medium. Because spherical symmetry exists, only variations in r are allowed, so the particle velocity is given by

$$v(r,t) = \nabla\phi = \partial\phi/\partial r = \partial[1/r)f(t - r/c)]/\partial r$$

$$= -(1/r^2)f(t - r/c) - (1/rc)f'(t - r/c). \tag{A6}$$

Taking the Fourier transform of Eq. (A6) yields

$$V(r,f) = -(1/r^2)F(f)e^{-j\omega r/c} - (j\omega/rc)F(f)e^{-j\omega r/c}, \tag{A7}$$

where F(f) is the Fourier transform of f(t). The volume velocity of the particles at a range r_0 (assuming spherical symmetry) is given by

$$Q(r_0,f) = 4\pi r_0^2 V(r_0,f)$$

$$= -4\pi F(f)e^{-j\omega r_0/c}(1 + j\omega r_0/c). \tag{A8}$$

Assuming that $\omega r_0/c \ll 1$, so that $e^{j\omega r_0/c} \doteq 1 + j\omega r_0/c$, then

$$Q(r_0,f) \doteq Q(f) = -4\pi F(f),$$

or

$$F(f) = -(1/4\pi)Q(f). \tag{A9}$$

The Fourier transform of $f(t)$ in the velocity potential then is defined by the Fourier transform of the volume velocity of the radiating surface of the transducer. From Eqs. (A5), the pressure at range r is given by

$$p(r,t) = -\rho_0\dot{\phi} = -(\rho_0/r)f'(t - r/c). \tag{A10}$$

Taking the Fourier transform of Eq. (A10) yields

$$P(r,f) = -(j\omega\rho_0/r)F(f)e^{-j\omega r/c}. \tag{A11}$$

Combining Eqs. (A9) and (A11) yields

$$P(r,f) = (j\omega\rho_0/4\pi r)Q(f)e^{-j\omega r/c}$$

$$= j(f\rho_0/2r)Q(f)e^{-j\omega r/c}. \tag{A12}$$

Substituting Eq. (A12) into Eq. (A2) yields

$$\frac{E(f)}{P(r,f)/j(f\rho_0/2r)e^{-j\omega r/c}} = \frac{P(f)}{I(f)},$$

or

$$\frac{E(f)}{P(f)} = -j(2r/f\rho_0)e^{+j\omega r/c}\,\frac{P(r,f)}{I(f)}. \tag{A13}$$

Because $E(f)/P(f)$ is the complex receiving response (complex free-field voltage sensitivity) and $P(r,f)/I(f)$ is the complex transmitting current response, Eq. (A13) becomes

$$M_T(f) = J(f,r)S(f),$$

where

$$J(f,r) = -j(2r/f\rho_0)e^{j\omega r/c} \tag{A14}$$

is the complex spherical reciprocity parameter.

Under the assumption made, this complex spherical reciprocity parameter should be useable in a conventional reciprocity calibration procedure to determine the complex transmitting and receiving responses. For example, Bobber's [13] Eq. (2.16) would become

$$M_H(f) = \left[-j \frac{E_{TH}(f) E_{PH}(f)}{E_{PT}(f) I_T(f)} \frac{2d_1}{f\rho_0} e^{j\omega d_1/c} \right]^{\frac{1}{2}}, \qquad \text{(A15)}$$

where d_1 is both the standard reference distance and the separation used for the calibration, and where $E_{TH}(f)$ is the Fourier transform (FT) of the hydrophone voltage output with the reciprocal transducer projecting, $E_{PT}(f)$ is the FT of the reciprocal transducer voltage output with the projector transmitting, $E_{PH}(f)$ is the FT of the hydrophone voltage output with the projector transmitting, and $I_T(f)$ is the FT of the driving current for the reciprocal transducer.

Appendix B

DERIVATION OF A MODIFIED RICIAN PROBABILITY DISTRIBUTION

A useful probability density function for acoustic calibration (using c-w sinusoidal waves) and for error analysis in the frequency domain is the distribution of the envelope of a sinusoidal signal contaminated by a zero-mean Gaussian noise. This function, often referred to as a Rician distribution, has the form

$$p(u) = (u/\sigma^2)\{\exp[-(u^2 + A^2)/2\sigma^2]\}I_0(uA/\sigma^2), \tag{B1}$$

where u is the peak-to-zero amplitude of the envelope, A is the peak-to-zero amplitude of the sinusoidal wave, σ^2 is the variance of the contaminating noise, and $I_0(uA/\sigma^2)$ is the modified Bessel function of zero order with argument (uA/σ^2). This expression is really a conditional probability of u, given A and σ^2. Although this probability is very useful, particularly in error analysis, it often is more desirable to have the conditional probability of A, given a measured value of the envelope and the noise statistic. This conditional probability could be useful in parameter estimation and the setting of confidence limits in the type of problem for which the objective is to estimate the level of a sinusoidal wave contaminated by noise. This probability density function may exist in the literature, but it has not been readily located; therefore, a derivation follows. The function will be referred to as a modified Rician distribution because of its close similarity to the Rician distribution.

Consider Figs. B1(a) and B1(b), which depict the geometries associated with the desired conditional probability. In both cases, x is a sample taken from a Rayleigh distribution so that

$$p(x) = (x/\sigma^2)\exp(-x^2/2\sigma^2). \tag{B2}$$

A Rayleigh distribution describes the envelope of a zero-mean Gaussian noise. Figure B1(a) represents the condition $u \geq x$; Fig. B1(b), the condition $u < x$. First, consider the condition depicted in Fig. B1(a). The conditional probabilities relating A and ϕ are

$$p(A|u,x)\,|dA| = p(\phi|u,x)\,|d\phi|,$$

or

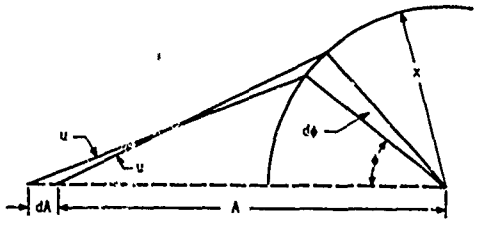

Fig. B1(a). Geometry associated with conditional probability of A, given u and x, with $u \geq x$; u is fixed; x is a sample from a Rayleigh distribution. $P(\phi|u,x;u\geq x) = 1/\pi$ for $\pi > \theta > 0$.

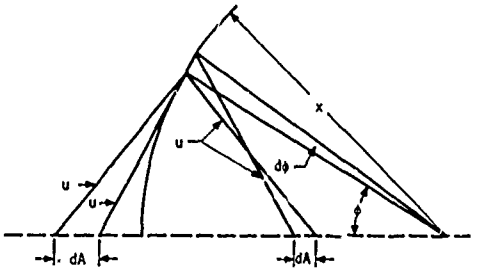

Fig. B1(b). Geometry associated with conditional probability of A, given x and u, with $u < x$; u is fixed. x is a sample from a Rayleigh distribution. $P(\phi|u,x;u<x) = 1/\arcsin(u/x)$ for $1/\arcsin(u/x) > \phi > 0$.

$$p(A|u,x) = \frac{p(\phi|u,x)}{\left|\frac{\partial A}{\partial \phi}\right|} . \tag{B3}$$

Now, for $u \geq x$, [see Fig. B1(a)],

$$p(\phi|u,x) = 1/\pi \tag{B4}$$

for $\pi \geq \phi \geq 0$. Also,

$$u^2 = x^2 + A^2 - 2Ax \cos \phi. \tag{B5}$$

Taking the partial derivative with respect to ϕ of both sides of Eq. (B5), with u and x constant, yields

$$0 = 2A(\partial A/\partial \phi) - 2x \cos \phi \, (\partial A/\partial \phi) + 2Ax \sin \phi,$$

or

$$\frac{\partial A}{\partial \phi} = \frac{2Ax \sin \phi}{2x \cos \phi - 2A} . \tag{B6}$$

From well-known trigonometric relations and from Eq. (B5),

$$\begin{aligned} 2Ax \sin \phi &= [(2Ax)^2 - (2Ax)^2 \cos^2 \phi]^{1/2} \\ &= [(2Ax)^2 - (A^2 + x^2 - u^2)^2]^{1/2} \\ &= \{[(A + u)^2 - x^2][x^2 - (A - u)^2]\}^{1/2}. \end{aligned} \tag{B7}$$

Also from Eq. (B5),

$$2x \cos \phi - 2A = (A + x^2 - u^2)/A - 2A$$

$$= (x^2 - u^2 - A^2)/A. \tag{B8}$$

Combining Eqs. (B6), (B7), and (B8) yields

$$\left|\frac{\partial A}{\partial \phi}\right| = \frac{A\{[(A + u)^2 - x^2][x^2 - (A - u)^2]\}^{\frac{1}{2}}}{|x^2 - u^2 - A^2|}. \tag{B9}$$

Combining Eqs. (B3), (B4), and (B9) yields

$$p(A|u,x;\ u \geq x) = \frac{1}{\pi} \frac{|x^2 - u^2 - A^2|}{A\{[(A + u)^2 - x^2][x^2 - (A - u)^2]\}^{\frac{1}{2}}}. \tag{B10}$$

In the case of Fig. B1(b), where $u < x$, A is a double-valued function of u and x; however, for any values of u and x, the probabilities of the two allowable values of A are the same, so that

$$p(A_1|u,x)\,|dA_1| = \tfrac{1}{2}p(\phi|u,x)\,|d\phi|,$$

$$p(A_2|u,x)\,|dA_2| = \tfrac{1}{2}p(\phi|u,x)\,|d\phi|. \tag{B11}$$

Because A_1 and A_2 do not occur at the same time and, for a given value of u, A_1 and A_2 are contiguous sets, it follows that for the condition where $u < x$, Eq. (B11) can be rewritten simply as

$$p(A|u,x)\,|dA| = \tfrac{1}{2}p(\phi|u,x)\,|d\phi|. \tag{B12}$$

The probability density of ϕ, given u and x, where $u < x$, is

$$p(\phi|u,x;u<x) = [\arcsin(u/x)]^{-1}. \tag{B13}$$

Because the derivation of $|\partial A/\partial \phi|$ is independent of conditions on u and x, Eqs. (B9), (B12), and (B13) may be combined to give

$$p(A|u,x;u<x) = \frac{1}{2 \arcsin(u/x)} \frac{|x^2 - u^2 - A^2|}{A\{[(A + u)^2 - x^2][x^2 - (A - u)^2]\}^{\frac{1}{2}}}. \tag{B14}$$

Equations (B10) and (B14) may be combined to give

$$p(A|u,x) = Q(u,x) \frac{|x^2 - u^2 - A^2|}{A\{[(A + u)^2 - x^2][x^2 - (A - u)^2]\}^{\frac{1}{2}}}, \tag{B15}$$

where

$$Q(u,x) = 1/[2 \arcsin(u/x)] \text{ for } u < x,$$

$$= 1/\pi \text{ for } u \geq x.$$

Now the joint probability density of A and x, given u, is

$$p(A,x|u) = p(A|u,x)p(x). \tag{B16}$$

Also,

$$p(A|u) = \int_{|u-A|}^{u+A} p(A,x|u)\,dx, \tag{B17}$$

where the upper and lower limits of the integral represent obvious upper and lower allowable limits of x for a given u and A. Combining Eqs. (B2), (B15), (B16), and (B17) yields

$$p(A|u) = \int_{|u-A|}^{u+A} Q(u,x)\,\frac{|x^2 - u^2 - A^2|}{A\{[(A+u)^2 - x^2][x^2 - (A-u)^2]\}^{1/2}} \times \frac{x}{\sigma^2}\exp(-x^2/2\sigma^2)\,dx \tag{B18}$$

where

$$Q(u,x) = 1/[2\arcsin(u/x)] \text{ for } u < x$$
$$= 1/\pi \text{ for } u \geq x.$$

To simplify Eq. (B18), let $x^2 = y^2 + (A-u)^2$. Then $y\,dy = x\,dx$ and

$$p(A|u) = \int_0^{2\sqrt{Au}} Q(u,y,A)\,\frac{|y^2 - 2Au|\,y}{Ay(4Au - y^2)^{1/2}}\,\frac{\exp\{-[y^2 + (A-u)^2]/2\sigma^2\}}{\sigma^2}\,dy, \tag{B19}$$

where

$$Q(u,y,A) = 2\{\arcsin u/[y^2 + (a-u)^2]\}^{-1} \text{ for } u < (y^2 + A^2)/2A$$
$$= 1/\pi \text{ for } u \geq (y^2 + A^2)/2A.$$

If we set $y = 2\sqrt{Au}\sin\theta$, then $dy = 2\sqrt{Au}\cos\theta\,d\theta$, and Eq. (B19) becomes

$$p(A|u) = \int_0^{\frac{1}{2}\pi} Q(u,\theta,A)\,\frac{2Au|\cos 2\theta|}{A\sqrt{4Au}\,\sigma^2\cos\theta}\left\{\exp - \frac{4Au\sin^2\theta + (A-u)^2}{2\sigma^2}\right\} \times (2\sqrt{Au}\cos\theta)\,d\theta$$

$$= 2(u/\sigma^2)\exp[-(A-u)^2/2\sigma^2]\int_0^{\frac{1}{2}\pi} Q(u,\theta,A)\,|\cos 2\theta| \times \exp\left(\frac{-2Au}{\sigma^2}\sin^2\theta\right)d\theta. \tag{B20}$$

where

$$Q(u,\theta,A) = \{2 \arcsin[u/(u^2 + A^2 - 2Au \cos 2\theta)^{\frac{1}{2}}]\}^{-1} \text{ for } \cos 2\theta < A/2u$$

$$= 1/\pi \text{ for } \cos 2\theta \geq A/2u.$$

Equation (B20) is the desired conditional probability density function that should be of most use in parameter estimation and in the determination of confidence limits associated with the estimate. It is referred to in this report as a modified Rician distribution because of its similarity with the Rician distribution expressed in the form of Eq. (32) of the main text. Plots of the distribution are shown in Fig. B2 for $\sigma = 1$ and $u = 1,3,5$. Note the similarity between the modified Rician and the Rician (Fig. 2 of main text) for $u = 5$ and for $A = 5$. Both of these distributions approach the Gaussian distribution for large values of u and A.

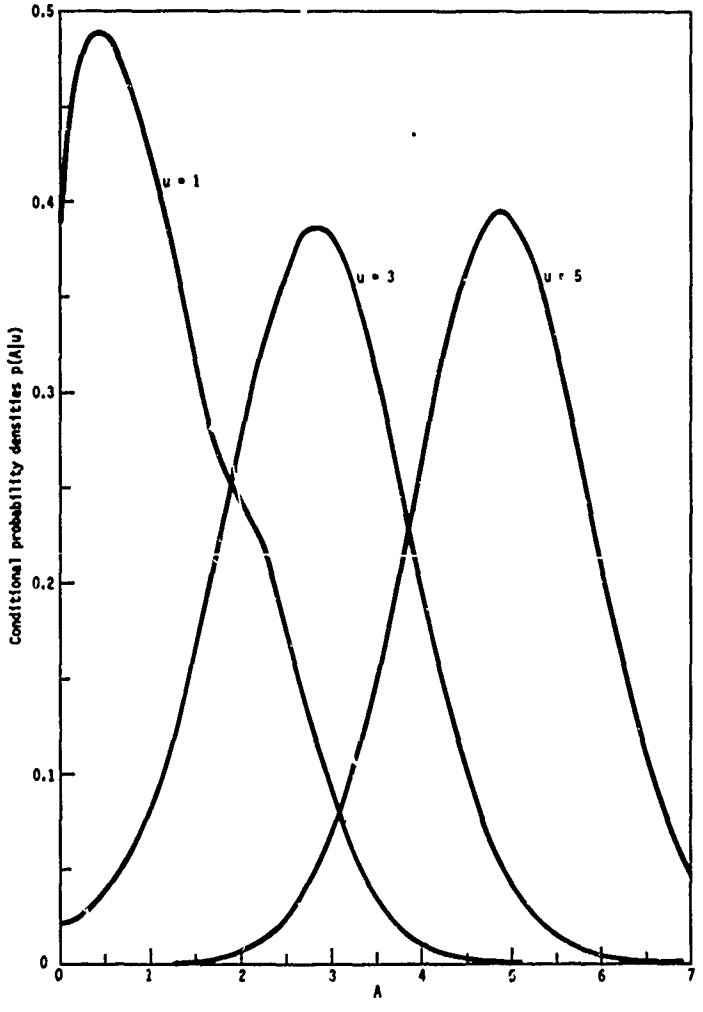

Fig. B2. Modified Rician probability densities for $\sigma = 1$ and $u = 1,3,5$.

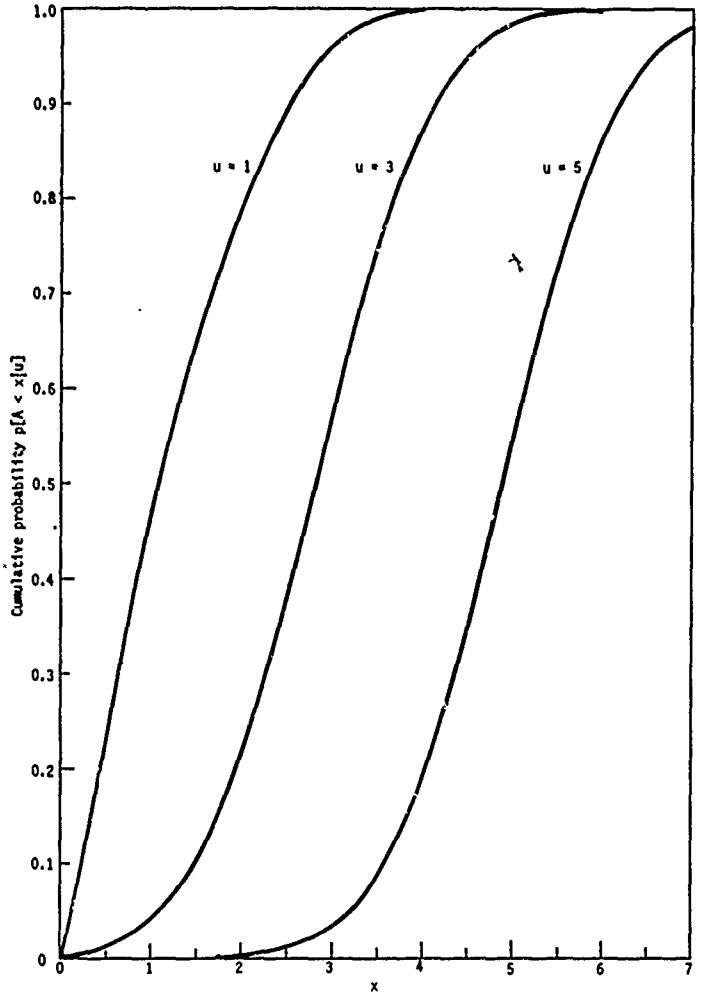

Fig. B3. Cumulative form of modified Rician distribution for $\sigma = 1$ and $u = 1,3,5$.

In determining the confidence limits associated with an estimate of A, given u, the cumulative form of the modified Rician distribution is desired. This is given by

$$p(A<x|u) = \int_0^x p(A|u)\,da, \tag{B21}$$

where $p(A|u)$ is given by Eq. (B20). Plots of the cumulative distribution are shown in Fig. B3 for $\sigma = 1$ and $u = 1,3,5$. An illustration of the use of this curve is as follows: Given $u = 3\sigma$, A has a probability of 0.21 of being less than 2σ and a probability of 0.13 of being greater than 4σ.

Another problem of some interest in regard to this report is the distribution of the quotient of two modified Rician variables. This quotient arises when the measured values of u_1 and u_2 are given along with the noise statistics σ_1^2 and σ_2^2 and it is desired to associate confidence

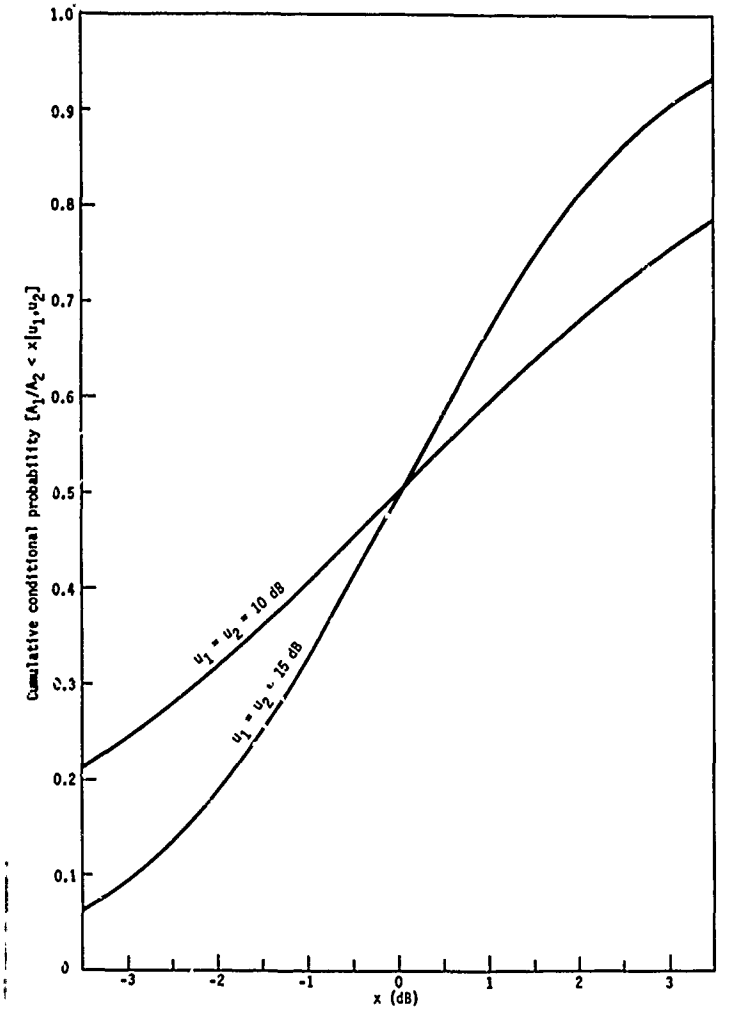

Fig. B4. Cumulative conditional probabilities of the quotient of two modified Rician variables; $\sigma_1 = \sigma_2 = 0$ dB.

limits to the estimate of A_1/A_2. The required cumulative distribution is given by

$$p[(A_1/A_2) < x|u_1,u_2] = \int_0^\infty p(A_2|u_2)\left[\int_0^{xA_2} p(A_1|u_1)dA_1\right]dA_2, \qquad (B22)$$

where the probability densities under the integral signs are given by Eq. (B20). Plots of this distribution are shown in Fig. B4 where σ_1 is assumed equal to σ_2, where the variables are expressed in decibels, and where $\sigma_1 = \sigma_2 = 0$ dB. Values are plotted for $u_1 = u_2 = 10$ dB and 15 dB.

Appendix C

SOME PROPERTIES OF PSEUDORANDOM NOISE WAVEFORMS

One choice for a complex deterministic broadband waveform to be used for underwater acoustic calibration purposes is the pseudorandom noise (PN) waveform. The advantage of this type of waveform over a transient waveform is that it is continuous and therefore allows for higher signal-to-noise ratios with smaller peak levels of the signal. There are several types of configurations for the generation of PN sequences, but the one shown in Fig. C1 will be discussed here. The PN generator of the figure consists of a n-element shift register where the "state" of each element of the register is shifted to the succeeding element with the application of a shift pulse. The new state of the first element is determined by a comparison of the m-th and n-th elements prior to the shift pulse. If the states of the two elements are the same, the new state of the first element will be "one." If the two states are different, the new state of the first element will be "zero." The m-th element is chosen so that the shift register will occupy all states (except the state consisting of all "ones") during the consecutive applications of shift pulses. Sequences that occupy all such states often are called m-ary sequences. The logic described above for the determination of the new state for the first element of the register on receipt of a shift pulse may be expressed as

$$A_1' = A_m \cdot A_n \vee \bar{A}_m \cdot \bar{A}_n$$

$$= A_m \diamond A_n, \qquad \text{(C1)}$$

where the primed variable is the new state and the unprimed variable is the old state and the symbols have the following meanings:

$\cdot$ ≡ "and" function

$\vee$ ≡ "or" function

$\bar{\ }$ ≡ "not" function

$\diamond$ ≡ arbitrary short form for the logic of the equation.

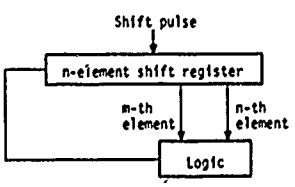

Fig. C1. Pseudorandom noise generator configuration.

Actually, the logic is the "not" of the "exclusive-or" function. It is also equivalent to the expression

$$A_1' = (1 + A_m + A_n)_{\text{modulo } 2}, \tag{C2}$$

where addition modulo 2 is zero for an even sum and one for an odd sum. Perhaps a clearer way to express the logic and one that is more significant to the development that follows is to allow the "one" state of an element to be represented by a voltage of +1 V and the zero state to be represented by -1 V. The logic then becomes simply

$$A_1' = A_m \times A_n. \tag{C3}$$

Actually, a complete m-ary sequence often may be derived through logic involving A_n and only one other element; however, m-ary sequences also may be derived by using more variables. Equation (C4) is an example of such use:

$$A_1' = A_i \times A_j \times A_k \times A_n. \tag{C4}$$

Necessary (but not sufficient) conditions on Eq. (C4) for a m-ary sequence are that an even number of variables be involved and A_n be one of the variables.

Another point of general interest about m-ary sequences is that where a complete sequence is obtained with a given combination of variables, a complete sequence also is available with a set of complementary variables. For example, if Eq. (C4) describes a logic that produces a complete sequence, then

$$A_1' = A_{n-i} \times A_{n-j} \times A_{m-k} \times A_n \tag{C5}$$

also will produce a complete sequence. This property is related to the unqualified capability of running a sequence either forward or backward.

Table C1 shows connections for PN generators with complete sequences. The number of states occupied by the shift register during a complete sequence is $(2^n - 1)$. As an illustrative example, Table C2 shows the sequential states occupied by a 5-element PN generator with m = 3.

The PN sequence usually observed is the change in state of the n-th element of the shift register. Using the +1 V and -1 V representation, the waveform representing the sequence from a 5-element PN generator (m = 3) is shown in Fig. C2. This waveform is periodic with a period corresponding to the time required for 31 $(2^5 - 1)$ shift pulses, assuming that the shift pulses are uniformly spaced. It is of interest to note that for the 5-element generator with m = 2, the output waveform would be identical except for an inversion in time.

Table C1. Connections for complete PN sequences.

Number of elements	Taps for complete sequence	Length of sequence
4	1,3	15
5	2,3	31
6	1,5	63
7	1,3,4,6	127
8*	(1:6:7),(1:2:7)	255
9	4,5	511
10	3,7	1023
11	2,9	2047
12*	(4:10:11),(1:2:8)	4095
13*	(8:11:12),(1:2:5)	8191
14*	(2:12:13),(1:2:12)	16383
15	1,4,7,8,11,14	32767

*Two-parameter logic for a complete sequence is not available for this number of elements. One complementary set of 4-parameter logic that will produce the complete sequence is given, which is not to imply that other 4-parameter logic combinations do not exist.

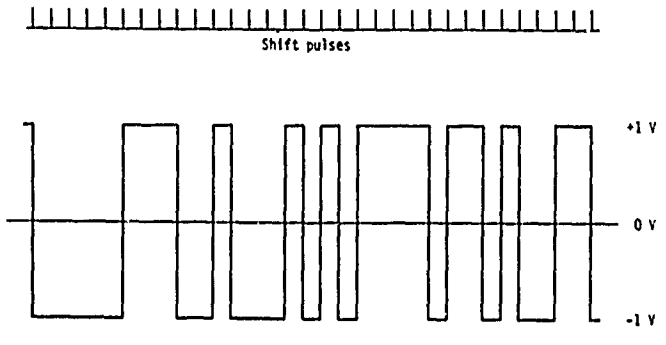

Fig. C2. Output voltage waveform for five-element PN generator (m = 3).

Table C2. Sequential states of 5-element PN generator (m = 3).

0.	00000	16.	11101
1.	10000	17.	11110
2.	11000	18.	01111
3.	11100	19.	10111
4.	01110	20.	11011
5.	00111	21.	01101
6.	10011	22.	10110
7.	01001	23.	01011
8.	00100	14.	00101
9.	00010	25.	10010
10.	10001	26.	11001
11.	01000	27.	01100
12.	10100	28.	00110
13.	01010	29.	00011
14.	10101	30.	00001
15.	11010	31.	00000

If g(t) is defined as the output waveform of the fifth element of the 5-element (m = 3) generator, then the output of the fourth element would be given by g(t - p), where p is the time interval between shift pulses. Likewise, the output of the first element would be given by g(t - 4p). If g(t - 5p) is desired, it may be obtained by applying the logic that is used to obtain the new state of the first element following a shift pulse. Since this is the product of the third and fifth elements of the register, this product is g(t - 5p). Any desired delay in integral increments of p may be obtained by following a similar logic. It should be obvious that this logic always will take the form of products of appropriate shift register elements. Note in Table C3 that all combinations of the five elements, taken one at a time, two at a time, three at a time, four at a time, and five at a time are required to provide the 31 different required delays. This same general condition exists for any length PN generator where the sequence is complete. That is,

$$\sum_{i=1}^{n} C_i^n = 2^n - 1, \tag{C6}$$

where C_i^n is the number of combinations of n things taken i at a time.

Table C3. Elements of 5-element PN generator (m = 3) to be multiplied to obtain indicated delay.

Delay	Appropriate elements*	Delay	Appropriate elements*
0	00001	16p	11011
p	00010	17p	10011
2p	00100	18p	00011
3p	01000	19p	00110
4p	10000	20p	01100
5p	00101	21p	11000
6p	01010	22p	10101
7p	10100	23p	01111
8p	01101	24p	11110
9p	11010	25p	11001
10p	10001	26p	10111
11p	00111	27p	01011
12p	01110	28p	10110
13p	11100	29p	01001
14p	11101	30p	10010
15p	11111	31p	00001

*Appropriate elements to be multiplied are indicated by 1's in elements to be used. For example, a delay of 10p is obtained by multiplying the outputs of the first and fifth elements (using +1 V and -1 V as the 1 and 0 states).

It follows from Eq. (C6) and the logic defined for determining desired delays of a given PN generator with a complete sequence that the product of a sequence by a delayed version of the sequence (where the delay is an integral number of shift intervals) is the same sequence, but with a different delay. That is,

$$g(t - jp)g(t - kp) = g(t - \ell p). \qquad \text{(C7)}$$

For example, from Table C3, if j = 0 and k = 15, then ℓ = 24. (*Note:* In the development of the logic when any element of the register is used an even number of times in the product, it has no effect on the output.) Likewise, if j = 1 and k = 16, then ℓ = 25. This is a very important

property of the PN sequence, because it gives a method for calculating the autocorrelation function and hence the power spectral density of the sequence. The autocorrelation function for a periodic PN signal then is given by

$$\phi(\tau) = (1/T) \int_{-T/2}^{T/2} g(t)g(t - \tau)dt,$$

or

$$\phi(kp) = (1/T) \int_{-T/2}^{T/2} g(t)g(t - kp), \tag{C8}$$

where T is the period of the PN sequence. If k = 0, then

$$\phi(0) = (1/T) \int_{-T/2}^{T/2} g^2(t)dt = 1. \tag{C9}$$

If $k \neq 0$, then from Eq. (C7),

$$\phi(kp) = (1/T) \int_{-T/2}^{T/2} g(t - \ell p). \tag{C10}$$

Because the PN sequence spends 2^{n-1} shift intervals in the "zero" state (or -1 V state) and $(2^{n-1} - 1)$ shift intervals in the "one" state (or +1 V state), then

$$\phi(kp) = -p/(2^n - 1)p = -1/(2^n - 1). \tag{C11}$$

Because the signal is periodic with a period of T, the autocorrelation function also will be periodic with a period of T. Because the sequence is a waveform with only two allowable states, the interpolation of $\phi(kp)$ for nonintegral values of k is a linear interpolation; that is

$$\phi(\tau) = -1/(2^n - 1) \text{ for } T/2 > |\tau| > p$$

$$= 1 - \frac{2^n}{2^n - 1} \frac{|\tau|}{p} \text{ for } p > |\tau| > 0. \tag{C12}$$

The autocorrelation function of a PN sequence is shown plotted in Fig. C3. For purposes of calculation, it is desirable to rewrite Eq. (C12) in the form

$$\phi(\tau) = K + \phi_0(\tau),$$

where $K = -(2^n - 1)^{-1}$, and

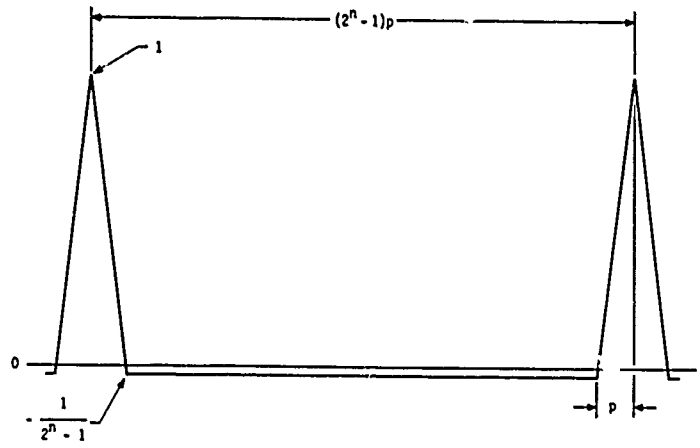

Fig. C3. Typical autocorrelation function of a PN sequence.

$$\phi_0(\tau) = \frac{2^n}{2^n - 1}\left(1 - \frac{|\tau|}{p}\right) \text{ for } p > |\tau| > 0$$

$$= 0 \text{ for } T/2 > |\tau| > p. \qquad \text{(C13)}$$

The K term in this equation is due to the d-c term in the PN sequence, which is due to the fact that the sequence spends one interval more in the "zero" state than it does in the "one" state. It should be obvious that with an appropriate adjustment of the voltage levels associated with the two states, Eq. (C12) may be rewritten

$$\phi(\tau) = 1 - |\tau|/p \text{ for } p > |\tau| > 0$$

$$= 0 \text{ for } T/2 > |\tau| > p. \qquad \text{(C14)}$$

If the PN sequence is considered to be very long so that T goes to infinity (or the harmonic components in the signal become infinitely close together), then the power spectral density of the sequence becomes

$$P(f) = \text{Fourier transform of } \phi(\tau)$$

$$= 2\int_0^p (1 - \tau/p)\cos \omega\tau \, d\tau$$

$$= p\left(\frac{\sin \pi fp}{\pi fp}\right)^2. \qquad \text{(C15)}$$

Equation (C15) actually represents the envelope of the powers associated with the various harmonics of the PN signal. It is interesting to note that the power spectral density of Eq. (C15) is relatively flat for frequencies below 1/4p (<1 dB) and that as p goes to zero, the power spectral density approaches that of a unit impulse function.

The advantages of a PN sequence for use in broadband calibration procedures are then as follows:

1. The PN sequence is broadband with a desirable power spectral distribution.

2. It has noise-like characteristics, but actually is deterministic and reproducible.

3. It may be reproduced with any desired delay.

4. It has only two states, which may very well reduce the problems associated with power amplification to one of power switching.